Beam Position Monitors for Circular Accelerators

4 Oct. 2012 IBIC2012, Tsukuba

S. Hiramatsu, KEK

Contents

- Electrostatic BPM pickups

    Beam induced charge distribution

    Finite boundary element method

- Signal processing

    sum-over-difference (Δ/Σ) of pickup electrode signals

    Log-ratio BPM

    AM-PM conversion processing

- Beam-based characterization of BPMs

    Beam-based alignment

    Beam-based gain calibration

    Resolution measurement by 3-BPM correlation

- Coupling impedance of BPM pickups

Beam trajectory

BPM pickups

beam trajectory
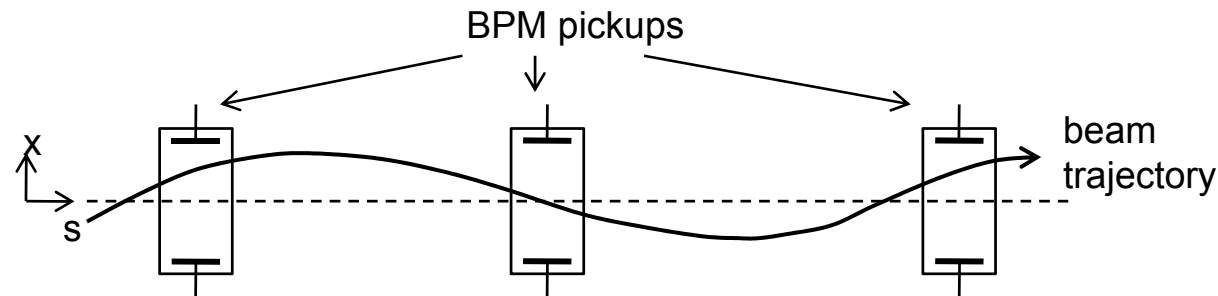
Measurement of closed orbit and/or betatron orbit with BPMs around accelerators gives beam optics parameters ($\beta(s)$, $\phi(s)$, $\eta(s)$ etc) .

Wideband BPM system measures betatron orbit:

$$x(s) = \sqrt{\varepsilon\beta(s)} \cos\nu\{\phi(s) - \phi_0\}$$

Narrow band BPM system measures closed orbit:

$$x(s) = \frac{\sqrt{\beta(s)}}{2\sin\pi\nu} \int\limits_s^{s+C} \sqrt{\beta(s')} \cos\{\pi\nu - \phi(s) + \phi(s')\} \frac{\Delta B(s)}{B\rho} ds'$$

Electrostatic pickup of BPM
- Beam induced charge on pickup electrode -

- The most popular BPM pickup consists of electrostatic induction pickup electrodes.

  hadron machine (long bunch)

  ---- a pair of parallel plates

  triangle cut pickup electrodes

  diagonal cut cylindrical electrodes
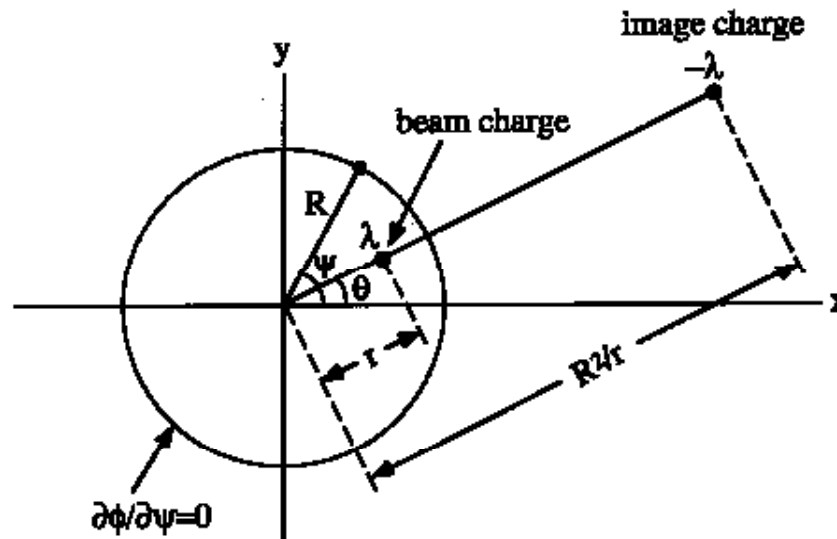
  etc.

  electron machine (short bunch)

  ---- button electrodes (2 buttons, 4 buttons)

Beam induced charge on the cylindrical pipe

Charge distribution on the pipe surface can be calculated by using mirror charge.

$$\sigma(R, \phi) = -\frac{\lambda}{2\pi R} \cdot \frac{R^2 - r^2}{R^2 + r^2 - 2rR\cos(\phi - \theta)}$$

$$= -\frac{\lambda}{2\pi R}\left\{1 + 2\sum_{n=1}^{\infty}\left(\frac{r}{R}\right)^n \cos n(\phi - \theta)\right\}$$

λ : line charge density of the pencil beam at (r, θ)

Beam induced charge on BPM electrodes with opening angle of ϕ_0

Induced charge on parallel-plate electrodes:

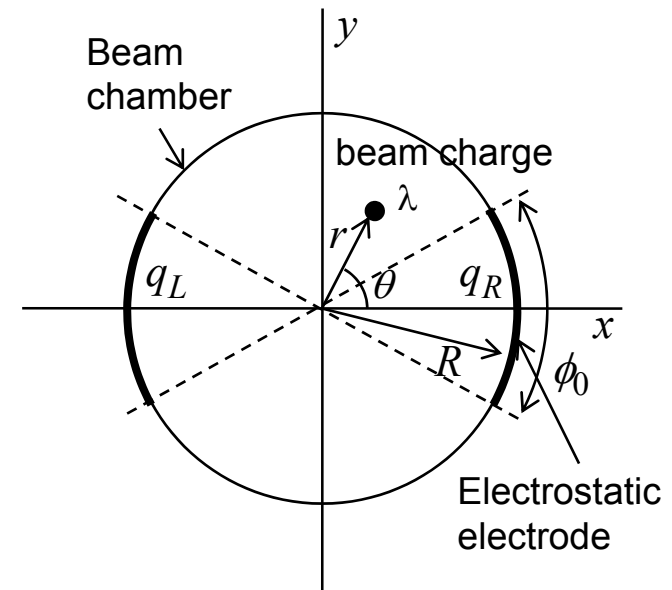$$q_R = \int_{-\phi_0/2}^{\phi_0/2} \sigma(R,\phi) R \, d\phi$$

$$= -\frac{\lambda}{2\pi}\left\{ \phi_0 + 4\sum_{n=1}^{\infty} \frac{1}{n}\left(\frac{r}{R}\right)^n \sin\left(\frac{n\phi_0}{2}\right)\cos n\theta \right\}$$

$$q_L = \int_{\pi-\phi_0/2}^{\pi+\phi_0/2} \sigma(R,\phi) R \, d\phi$$

$$= -\frac{\lambda}{2\pi}\left\{ \phi_0 + 4\sum_{n=1}^{\infty} \frac{1}{n}\left(\frac{r}{R}\right)^n \sin\left\{n\left(\pi + \frac{\phi_0}{2}\right)\right\}\cos n\theta \right\}$$

Induced signal voltages are expected to be :

$$V_R \propto q_R, \quad V_L \propto q_L$$

Δ/Σ ratio of signals of parallel pickup electrodes

Beam position:
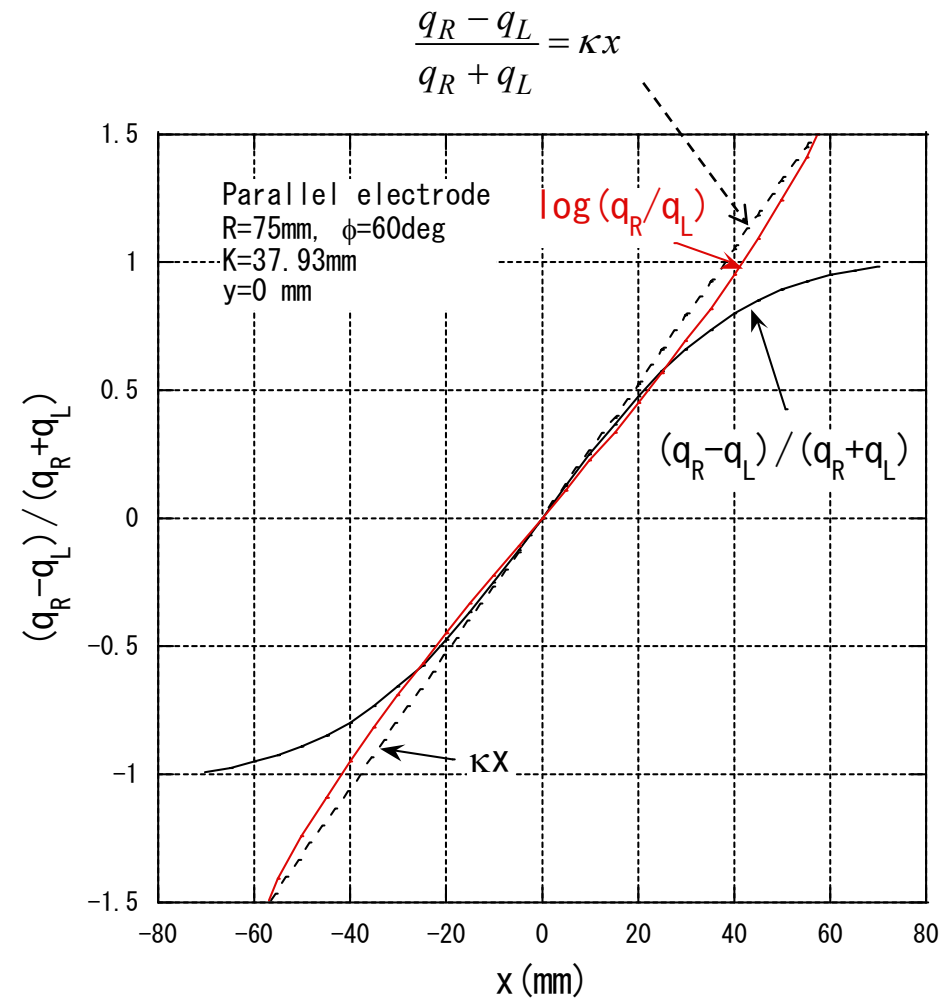
$$(x, y) = (r\cos\theta, r\sin\theta)$$

For x, y<<R

$$\frac{q_R - q_L}{q_R + q_L} = \kappa x$$

$$\kappa = \frac{2\sin(\phi_0/2)}{R\phi_0/2}$$

log(q$_R$/q$_L$) is more linear

than (q$_R$-q$_L$)/(q$_R$+q$_L$).

$$\frac{q_R - q_L}{q_R + q_L} = \kappa x$$

Parallel electrode
R=75mm, ϕ=60deg
K=37. 93mm
y=0 mm

$\log(q_R/q_L)$

$(q_R-q_L)/(q_R+q_L)$

κx

$(q_R-q_L)/(q_R+q_L)$

x (mm)

Calculation of beam induced charge with finite boundary element method

- For the case of the beam chamber with arbitrary shape cross section, the charge distribution induced on the chamber surface by the charged beam can be calculated using the finite boundary element method.

- The two dimensional potential $\phi(\boldsymbol{r})$ in the beam chamber is given by

$$\phi(\boldsymbol{r}) = \oint_{\text{surface}} \ln\left(\frac{1}{|\boldsymbol{r} - \boldsymbol{r}'(s)|}\right)\sigma(s)ds + \lambda\ln\left(\frac{1}{|\boldsymbol{r} - \boldsymbol{r}_0|}\right)$$

λ : line density of the beam charge (pencil beam) at $\boldsymbol{r}_0$

$\sigma(s)$: surface density of beam induced charge on the beam chamber

$\sigma(s)$ is given by solving the equation for $\phi(\boldsymbol{r}) = 0$ on the chamber surface.

Finite boundary element method (1)
for calculation of induced charge distribution

$$\oint_{\substack{\text{chmaber} \\ \text{surface}}} \ln\left(\frac{1}{|\mathbf{r} - \mathbf{r}'(s)|}\right)\sigma(s)ds = -\lambda \ln\left(\frac{1}{|\mathbf{r} - \mathbf{r}_0|}\right)$$

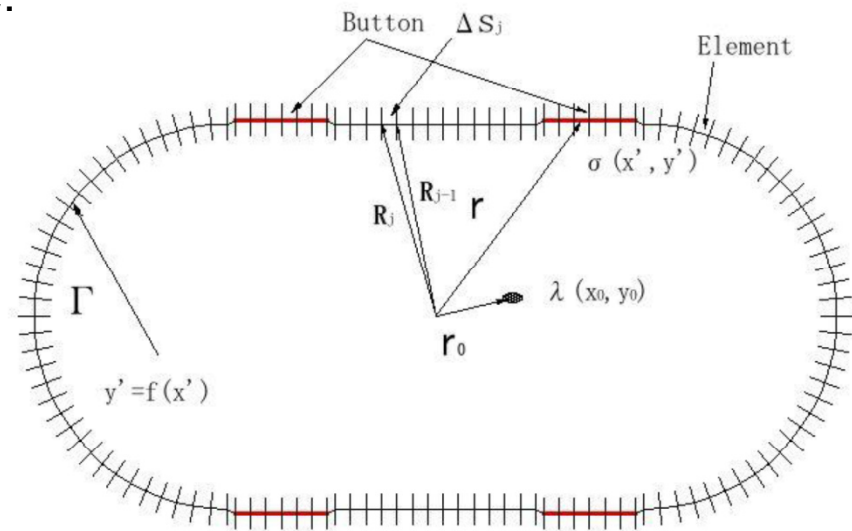The line integral is performed on the closed line along the cross section of the inner surface of the beam pipe.

Dividing boundary in small meshes:
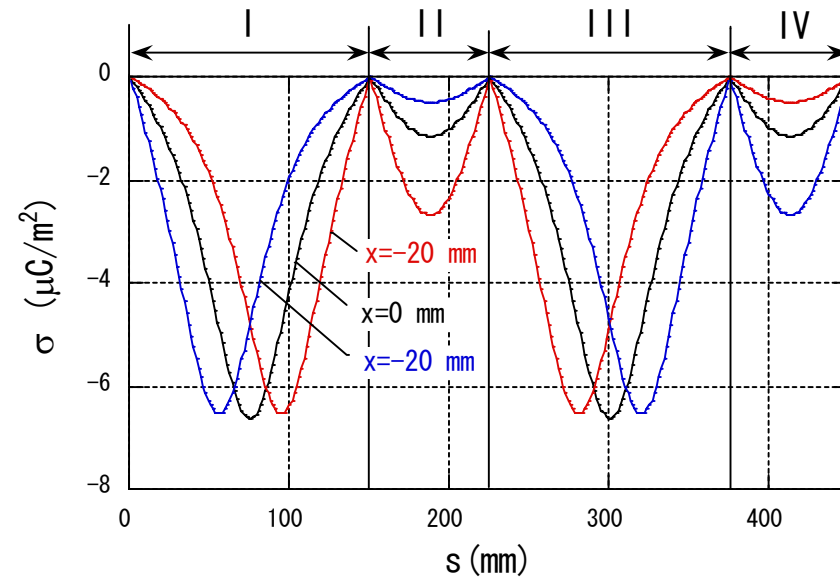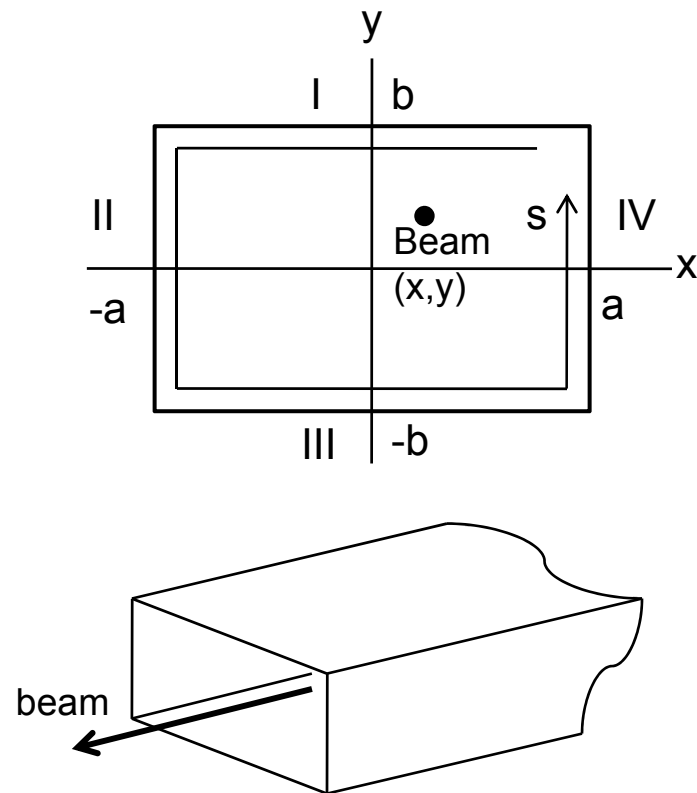
$$\boxed{\sum_j G_{ij}\sigma_j = -\lambda G_{i0}}$$

$$G_{ij} = \int_{\Delta s_j} \ln\left(\frac{1}{|\mathbf{r}_i - \mathbf{r}_j(s)|}\right)ds, \quad G_{io} = \ln\left(\frac{1}{|\mathbf{r}_0 - \mathbf{r}_i(s)|}\right)$$

λ : line charge density of pencil beam

σ_j : surface charge density on j-th element of the wall

Beam induced charge on the rectangular beam chamber
(finite boundary element method)

Beam Induced charge on triangle cut BPM electrodes
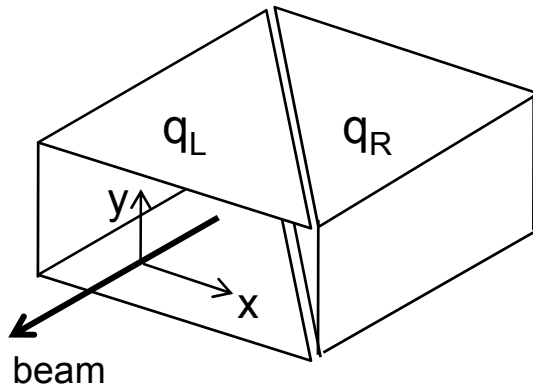
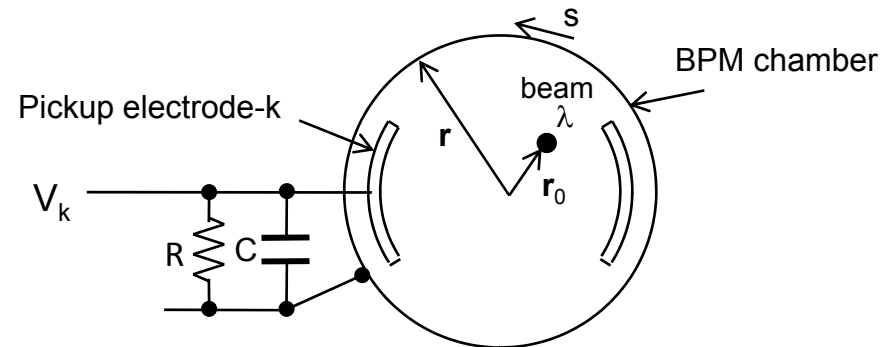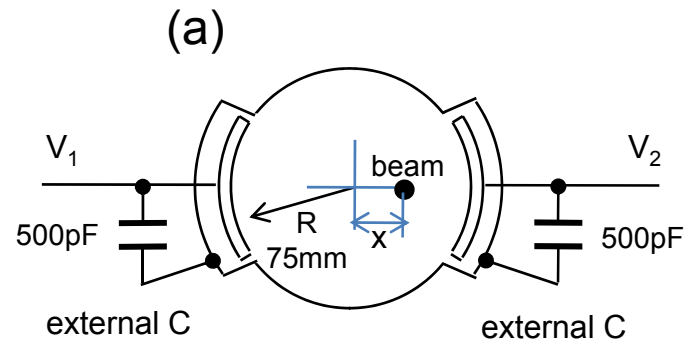$$q_i = \iint\limits_{electrode-i} \sigma(s)dsdz$$

$$\frac{q_R - q_L}{q_R + q_L} = \frac{x}{a}$$

TriangleElectrode

finite boundary element
(triangle electrode)

$-37.5mm < y_{beam} < 37.5mm$

$x = K\Delta/\Sigma$
$K = 75$ mm

Δ/Σ

x_{beam} (m)
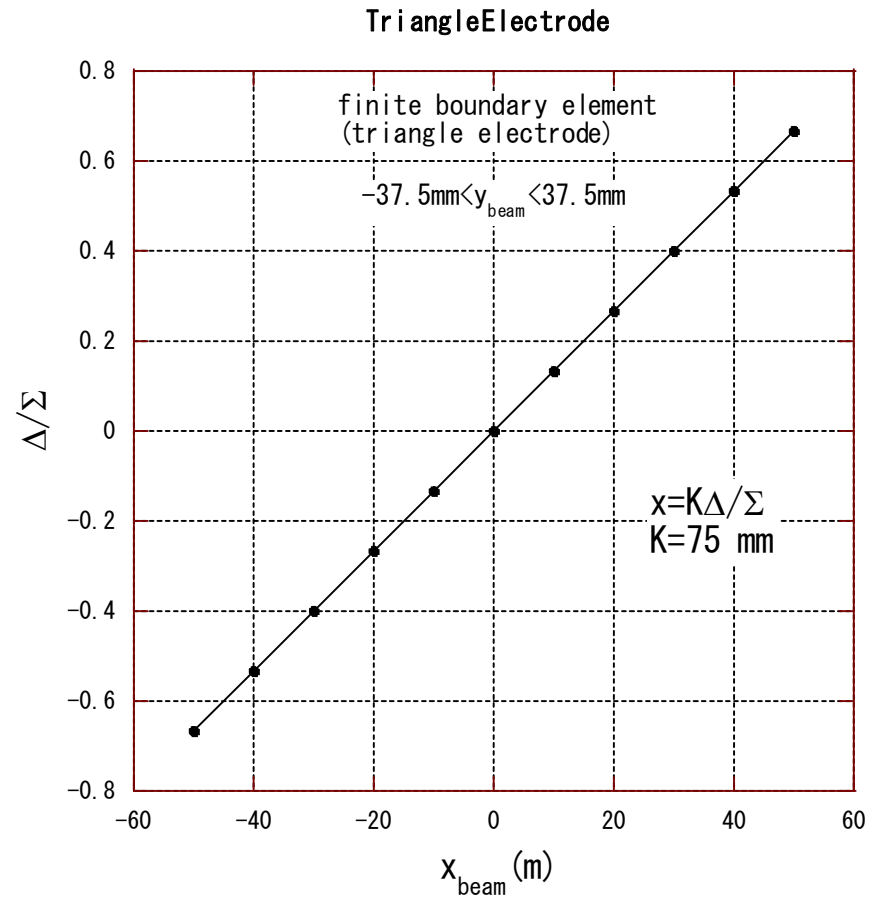
Finite boundary element method (2)

Induced harge distribution $\sigma(s)$ and pickup electrode potential V_k can be obtained simultaneously with finaite boundary element method.

For RC >> τ_b (bunch length in time),

$$\oint_{chmber} \ln\left(\frac{1}{|\boldsymbol{r}-\boldsymbol{r}'(s)|}\right)\sigma(s)ds = -\lambda\ln\left(\frac{1}{|\boldsymbol{r}-\boldsymbol{r}_0|}\right) \qquad (\boldsymbol{r}:\text{chamber surface})$$

$$\oint_{electrode\text{-}k} \ln\left(\frac{1}{|\boldsymbol{r}-\boldsymbol{r}'(s)|}\right)\sigma(s)ds + \lambda\ln\left(\frac{1}{|\boldsymbol{r}-\boldsymbol{r}_0|}\right) = 2\pi\varepsilon_0 V_k \qquad (\boldsymbol{r}:k\text{-}th\text{ electrode surface})$$

$$\oint_{electrode\text{-}k} \sigma(s)ds = -\frac{V_k}{C} \qquad (V_k:\text{electrode potential})$$

➡ $\sigma(s),\ V_k$ are determined by finite boundary element method

When we have gap between electrode and chamber,

κ becomes smaller than 2sin(ϕ/2)/(Rϕ/2)

(a)

V_1 beam V_2

R 75mm   x

500pF   500pF

external C   external C

$$\kappa \cong \frac{2\sin(\phi/2)}{R\phi/2}$$

(b)

85mm

V_1 beam V_2

R 75mm   x

500pF   500pF

external C   external C

$$\kappa < \frac{2\sin(\phi/2)}{R\phi/2}$$

x/K_x

$$(K_x = \frac{R\phi/2}{2\sin(\phi/2)})$$

y=0

D/S (2a)
D/S (2b)
DS0

(a)

(b)

10% decrease of κ

$(V_1-V_2)/(V_1+V_2)$

x (mm)
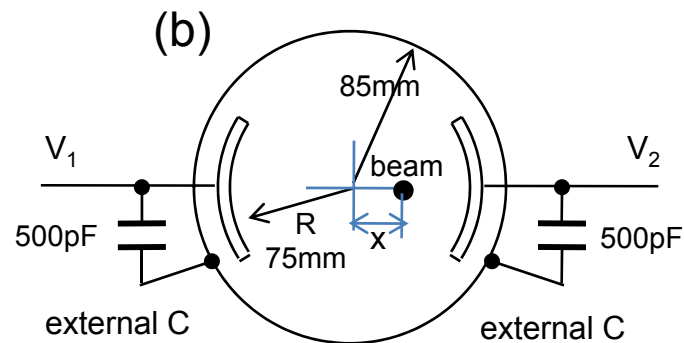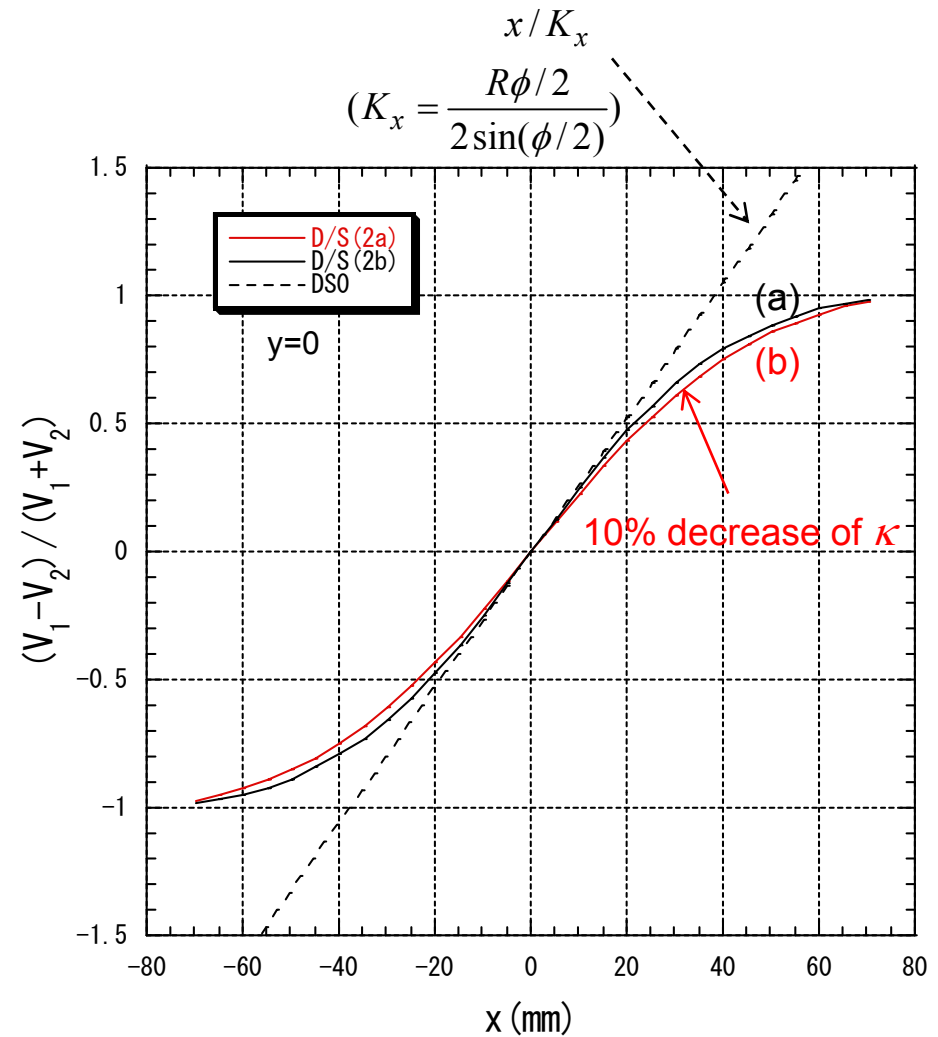
Beam induced charge on diagonal cut cylinder

Surface density of the beam induced charge
on the inner surface of the cylinder

$$\sigma(a,\phi) = -\frac{\lambda}{2\pi a} \cdot \frac{a^2 - r^2}{a^2 + r^2 - 2ar\cos(\phi - \theta)}$$

Induced charge on each diagonal cut electrode
has linear dependence on the beam position x (or y).

$$q_{\pm}(x,y) = \int_0^{2\pi} a\tan\theta(1\pm\cos\phi)\sigma(a,\phi;x,y)d\phi$$

$$= -\lambda\frac{L}{2}\left(1\pm\frac{x}{a}\right)$$
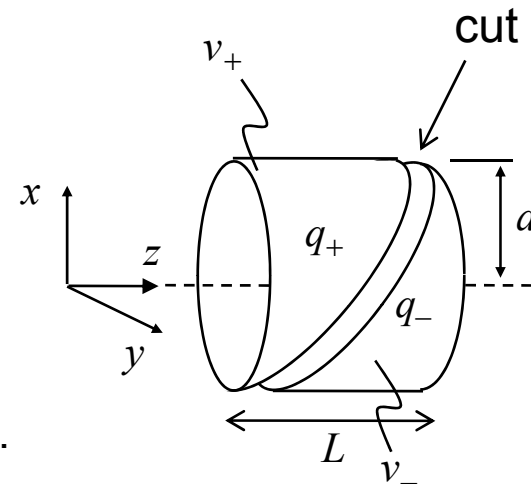
Coupling between electrodes
(diagonal cut BPM/J-Parc)

T. Toyama

C_{LR}

V_L R C_L i_L i_R C_R R V_R

V_U V_R

V_D V_L
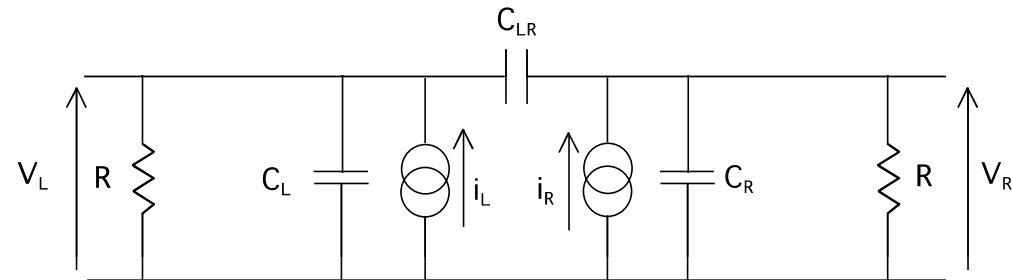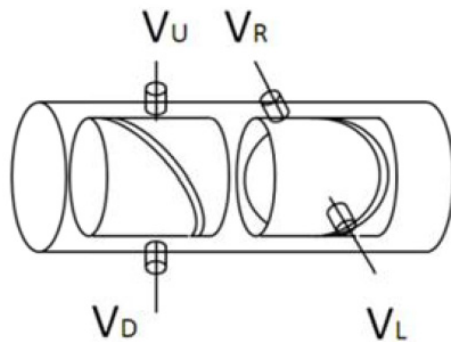
Mesured capacitance matrix (pF)

$$(C_{ij}) = \begin{pmatrix} 197.535 & -7.457 & -0.004 & -0.018 \\ -7.457 & 205.356 & -0.020 & -0.066 \\ -0.004 & -0.020 & 207.689 & -7.301 \\ -0.018 & -0.066 & -7.301 & 210.604 \end{pmatrix}$$
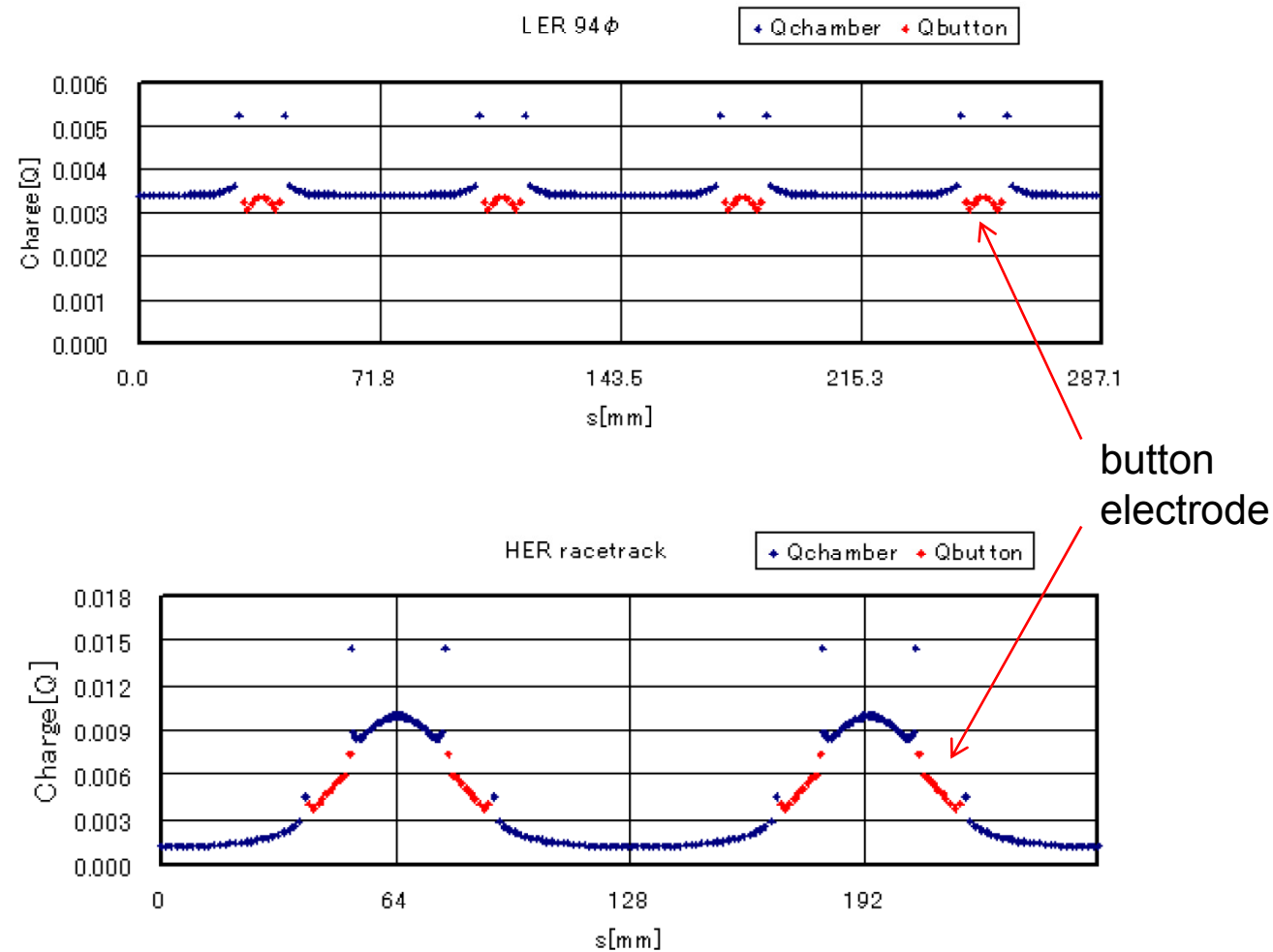
Frequency dependendce of κ $\left(\dfrac{L-R}{L+R} = \kappa x\right)$

Wire calibration

f_{RF}

Calculation

capacitive coupling between electrodes

IBIC2012, Tsukuba
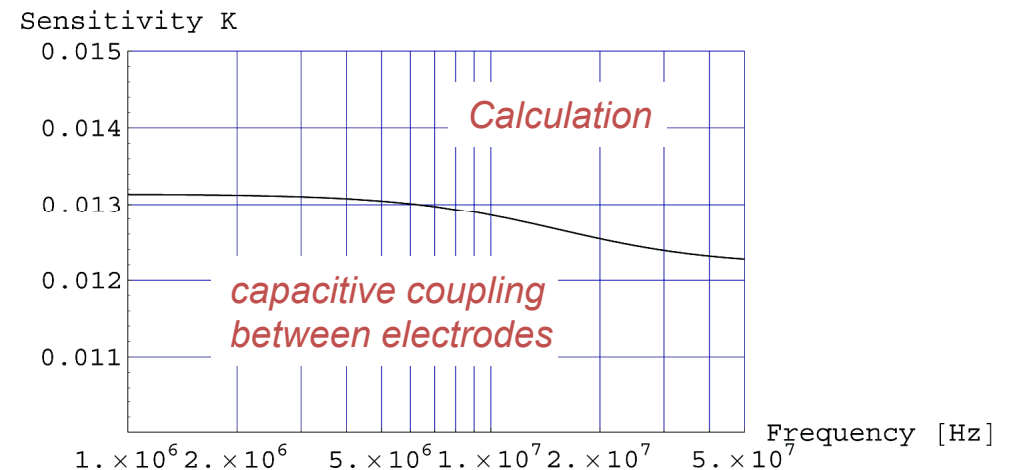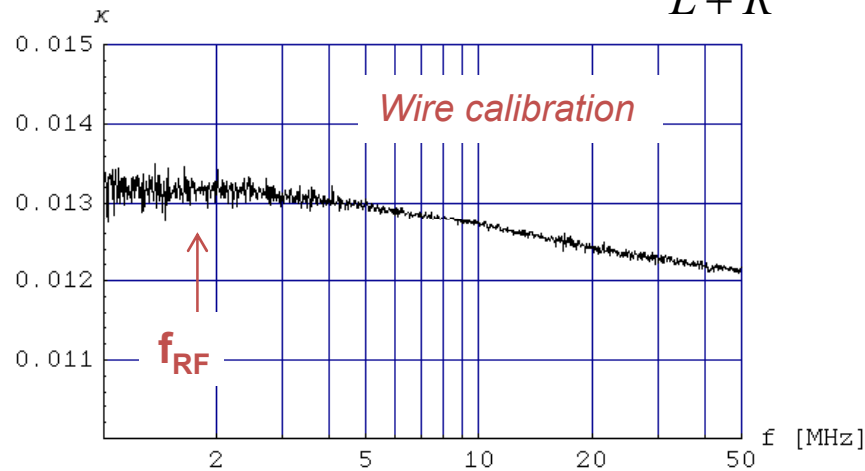
Charge distribution in the KEKB BPM pickup
(BPM with 4 button electrodes)

LER BPM   HER BPM
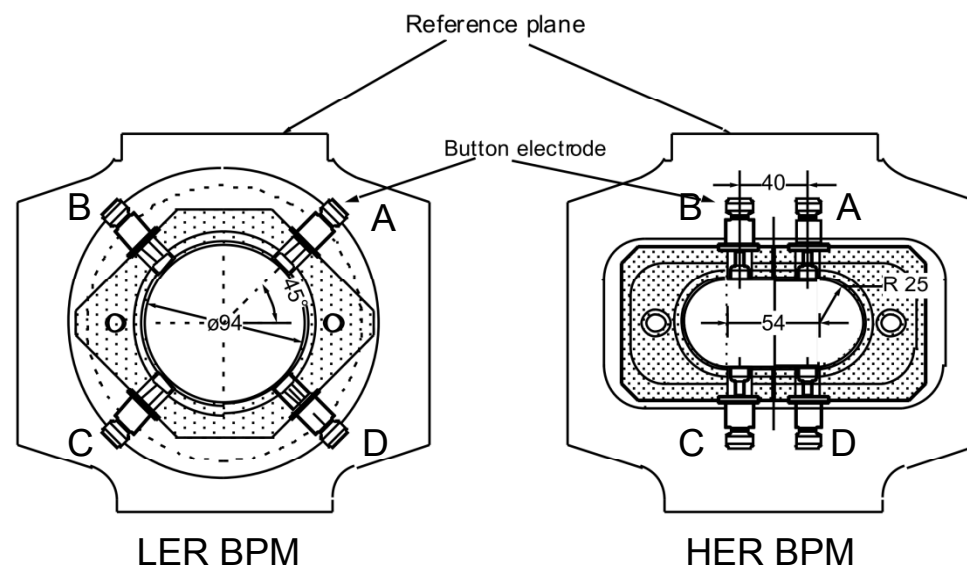
Mesh of finite boundary element method
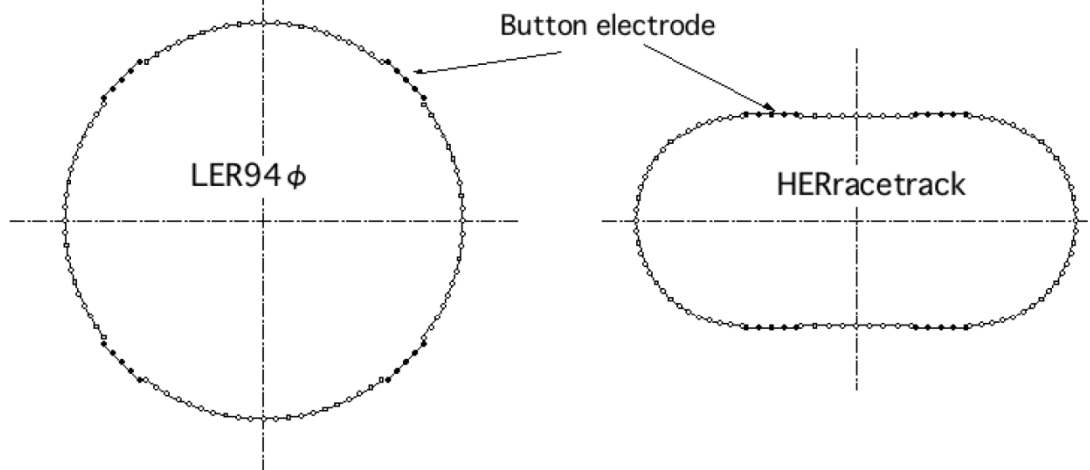
Calculated charge distribution by finite boundary element method

LER 94φ   • Qchamber • Qbutton

button electrode

HER racetrack   • Qchamber • Qbutton

Mapping of KEKB BPM calculated by finite boundary method

x=-10mm   LER94φ   x=10mm

y=10mm 0.4   y=10mm 0.6

(-10mm ≤ x, y ≤ 10mm)

$$\left\{ \begin{array}{l} X = \dfrac{A + D - B - C}{A + B + C + D} \\[2mm] Y = \dfrac{A + B - C - D}{A + B + C + D} \end{array} \right.$$

Mapping $\left\{ \begin{array}{l} x = F_x(X,Y) \\ y = F_y(X,Y) \end{array} \right.$
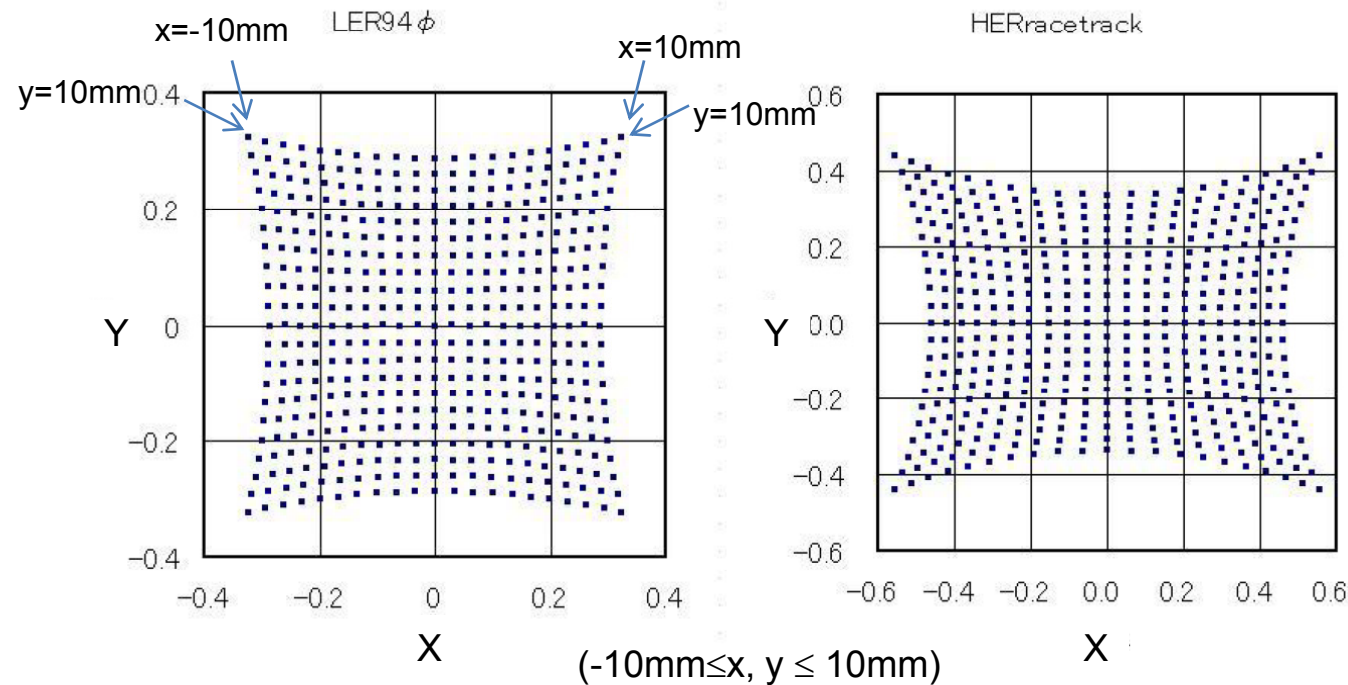
BPM calibration stand (wire method)
(J-Parc MR)

T. Toyama
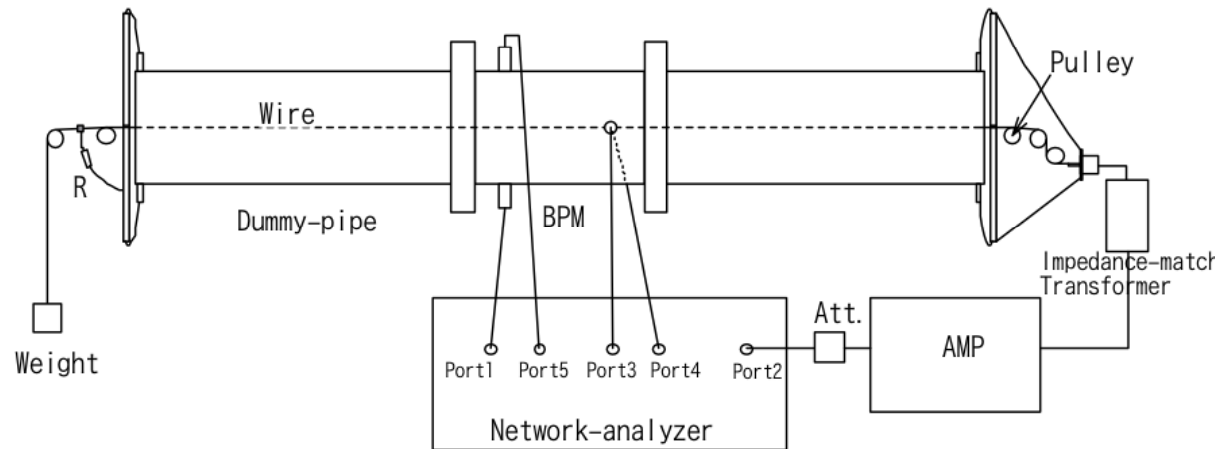
BPM electrode signal at wire calibration (diagonal cut BPM)

T. Toyama

Stretched wire current is not equivalent to the beam.
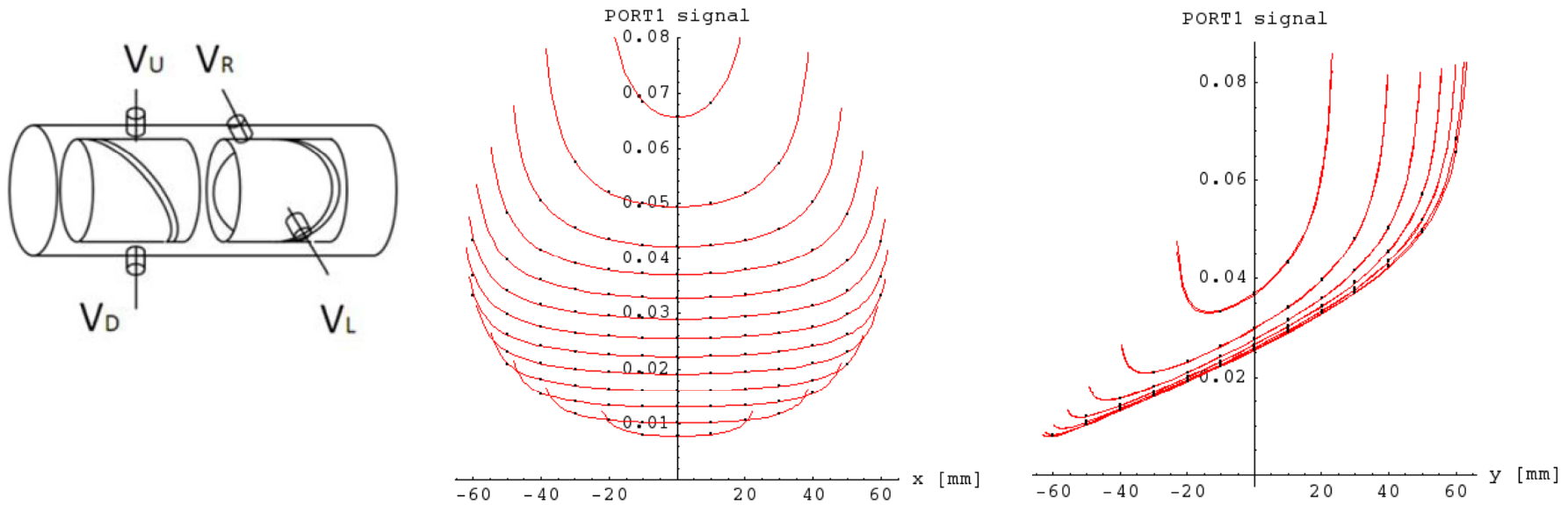
Signal of a diagonal cut electrode (upper electrode)

$$V_U(x, y) = V \frac{1 + \dfrac{y}{a}}{\cosh^{-1}\left(\dfrac{r_w^2 + a^2 - \left(x^2 + y^2\right)}{2 r_w a} \right)}$$

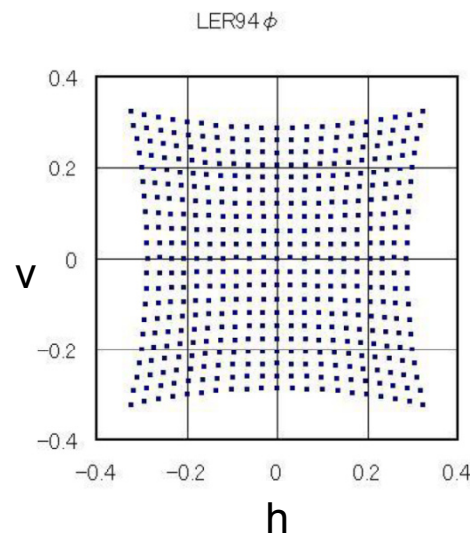Capacitance between wire and the pickup electrodes.
Canselled in Δ/Σ.

BPM mapping at calibration stand

BPM calibration stand (KEKB BPM)
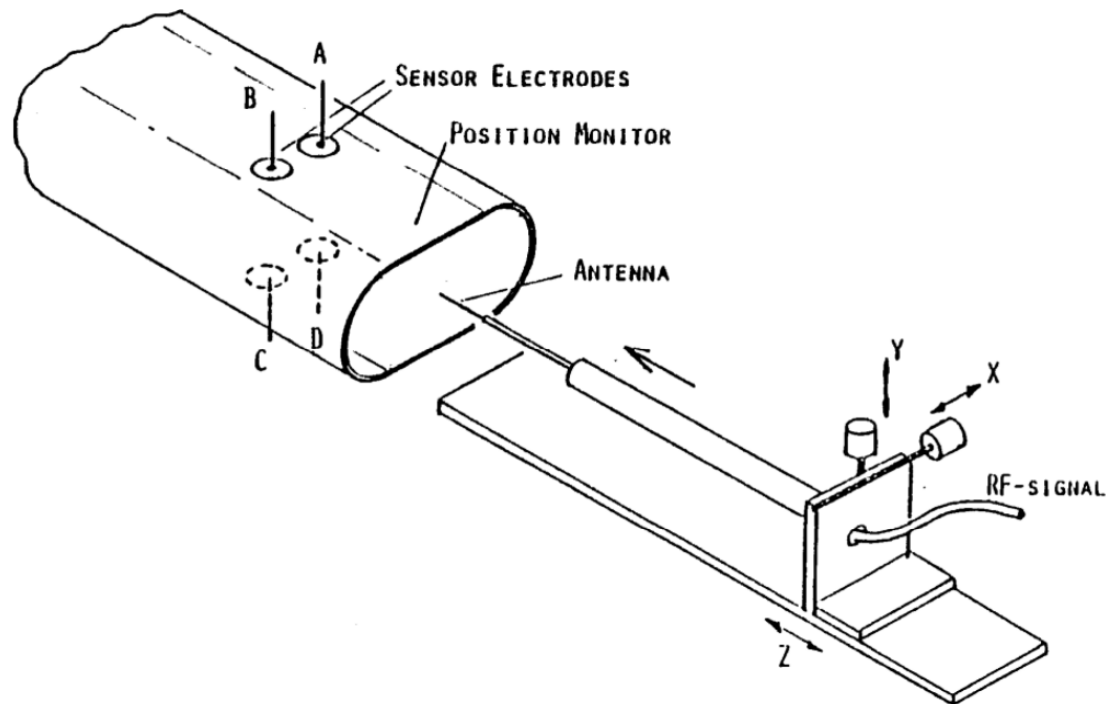
Correspondence between beam position and button signal : Mapping

$$h = \frac{V_1 + V_4 - V_2 - V_3}{V_1 + V_2 + V_3 + V_4}, \quad v = \frac{V_1 + V_2 - V_3 - V_4}{V_1 + V_2 + V_3 + V_4}$$
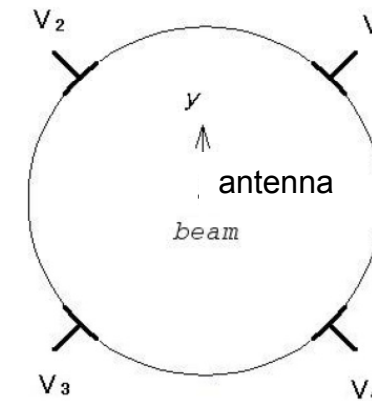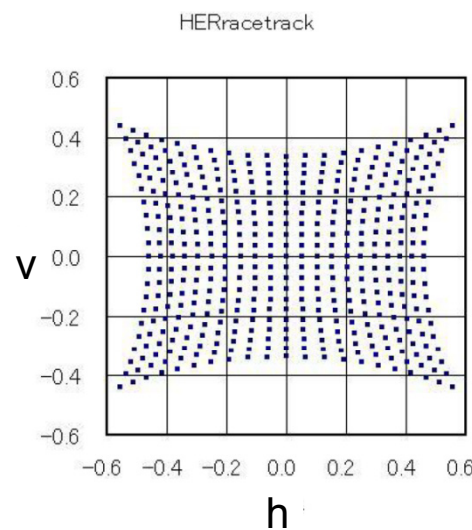
Antenna position
(beam position)
$$\begin{cases} x = F_x(h,v) \\ y = F_y(h,v) \end{cases}$$

$$F_x(h,v) = a_0 + a_1 h + a_2 v + a_3 h^2 + a_4 hv + a_5 v^2 + a_6 h^3 + a_7 h^2 v + a_8 hv^2 + a_9 v^3 + \cdots$$

$$F_y(h,v) = b_0 + b_1 h + b_2 v + b_3 h^2 + b_4 hv + b_5 v^2 + b_6 h^3 + b_7 h^2 v + b_8 hv^2 + b_9 v^3 + \cdots$$

a_i, b_i are determined by least squares to fit the measured mapping data.

Signal processing

Pickup response

BPM pickup

Equivalent circuit

Q : induced charge on pickup
electrode
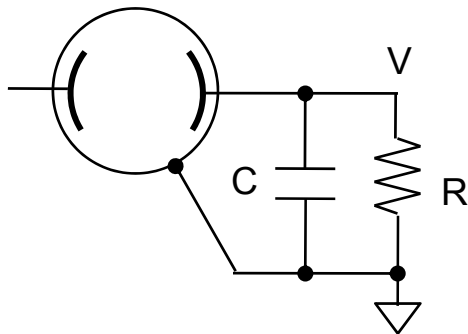
$$V(\omega) = \frac{j\omega CR}{1 + j\omega CR} \frac{Q(\omega)}{C}$$

Same response as HPF

Button electrode signal of KEKB BPM
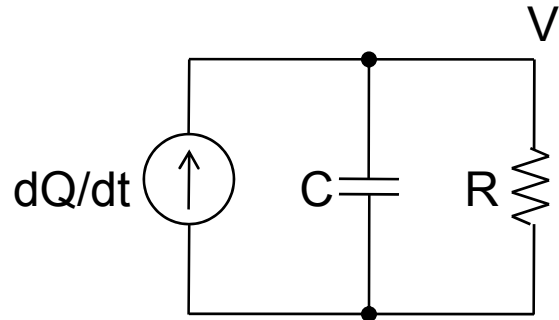(R=Z_0: cable impedance)
(observed through 100m coax cable)
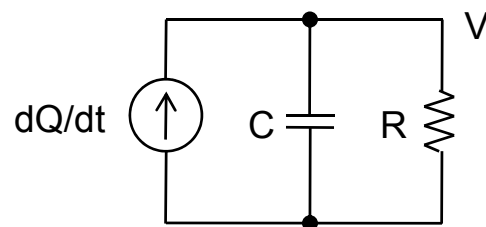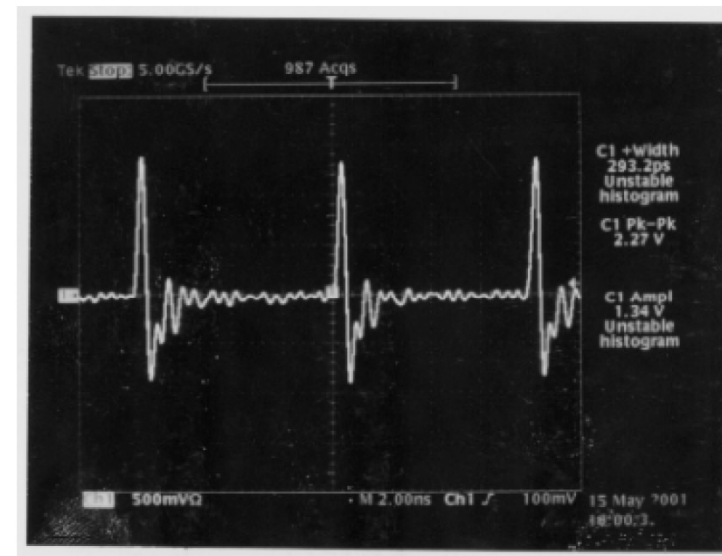
Capacitance of button electrode (KEKB)

M. Tejima

KEKB/LER BPM

V

dQ/dt C R

Single bunch beam

$$V(\omega) \sim \frac{j\omega CR}{1 + j\omega CR} e^{-\omega^2 \sigma_z^2 / c^2}$$

$$\omega \ll c / \sigma_z$$

$$|V(\omega)| \sim \frac{\omega CR}{\sqrt{1 + \omega^2 C^2 R^2}}$$

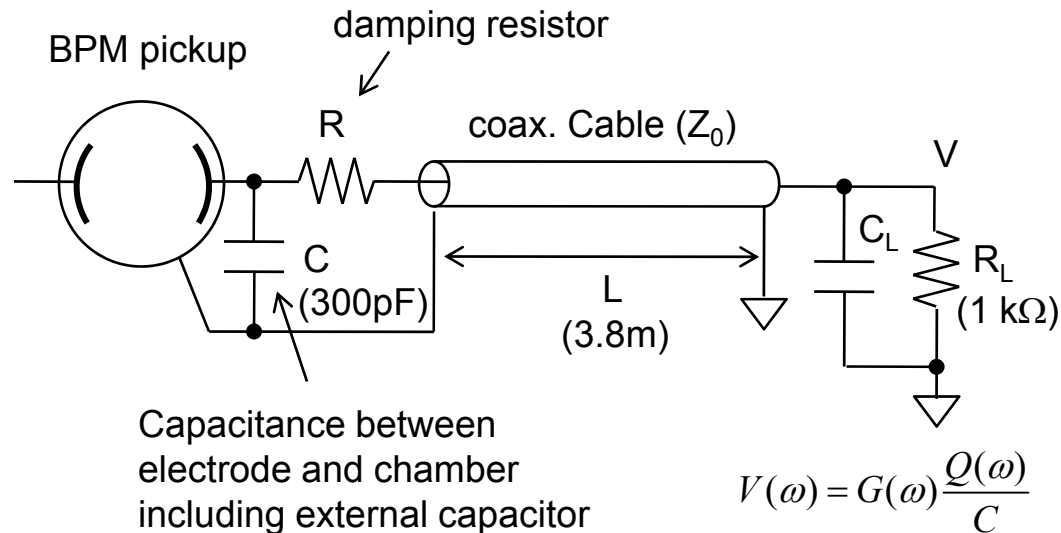C can be estimated from the signal spectrum obtained by single bunch operation.
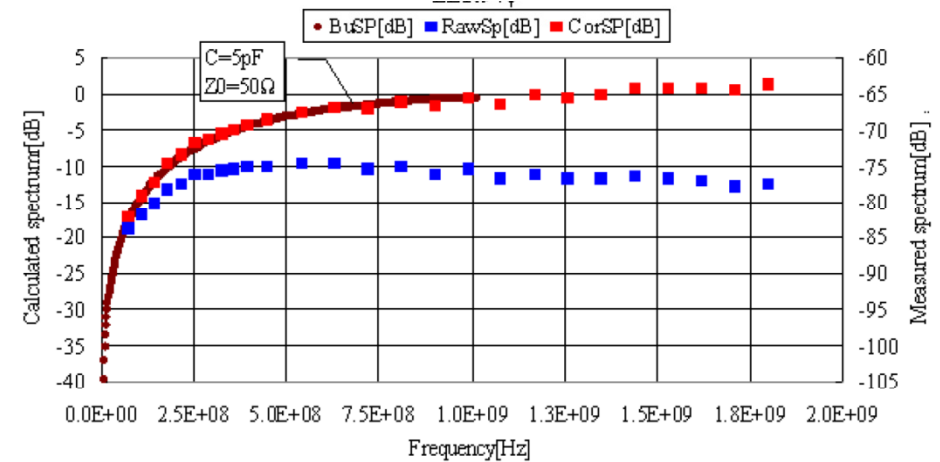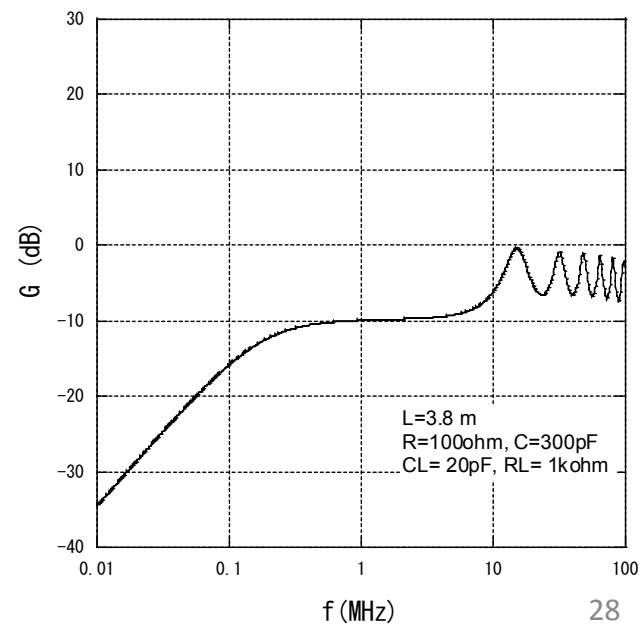

KEKB/HER BPM
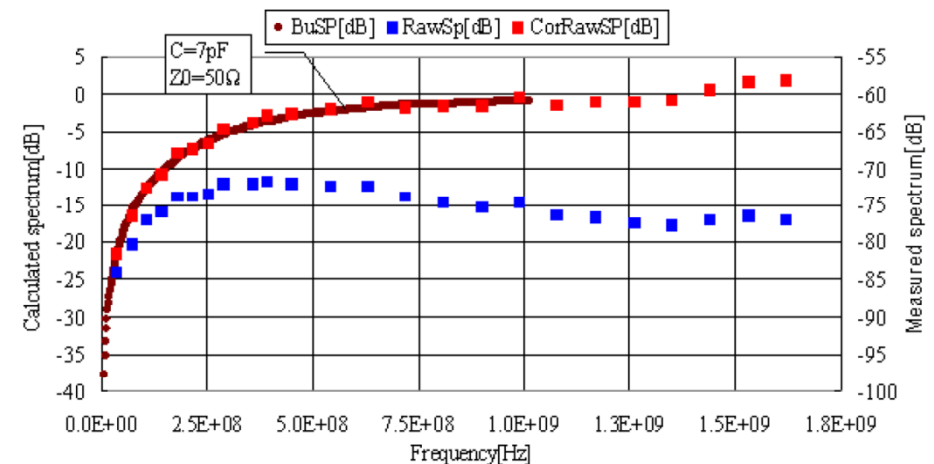
Resonance problem of signal cable

BPM pickup

damping resistor

R

coax. Cable (Z_0)

V

C
(300pF)

C_L

R_L
(1 kΩ)

L
(3.8m)

Capacitance between
electrode and chamber
including external capacitor
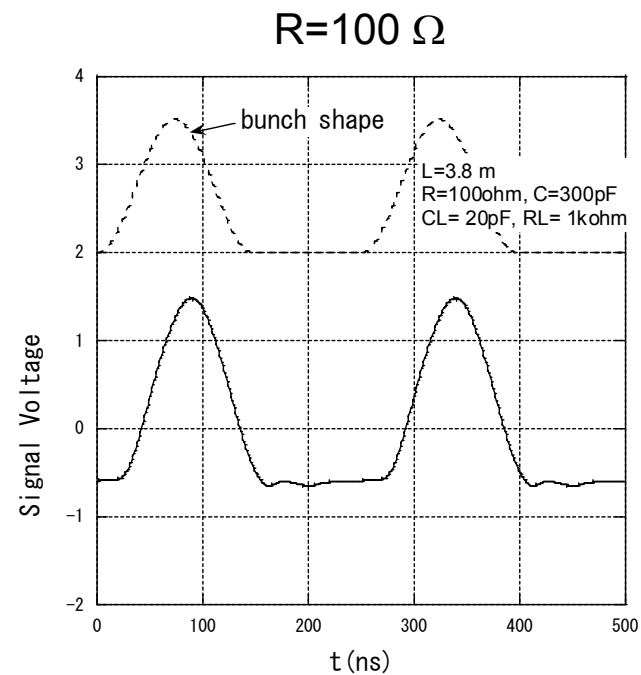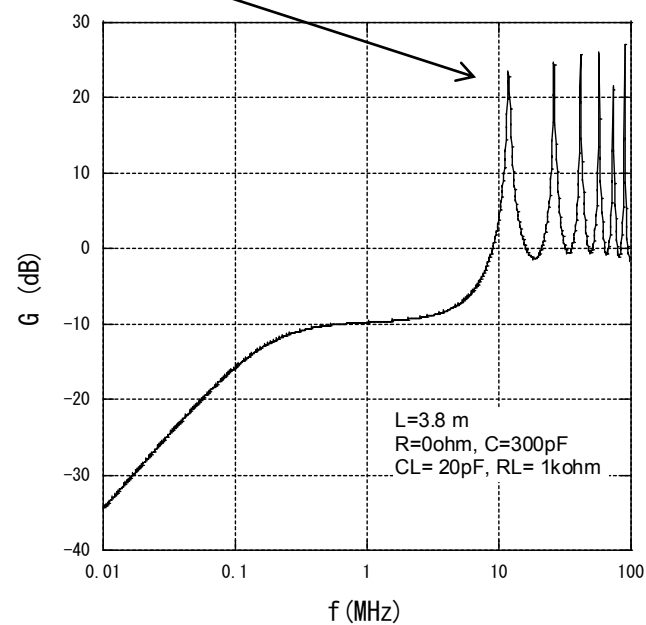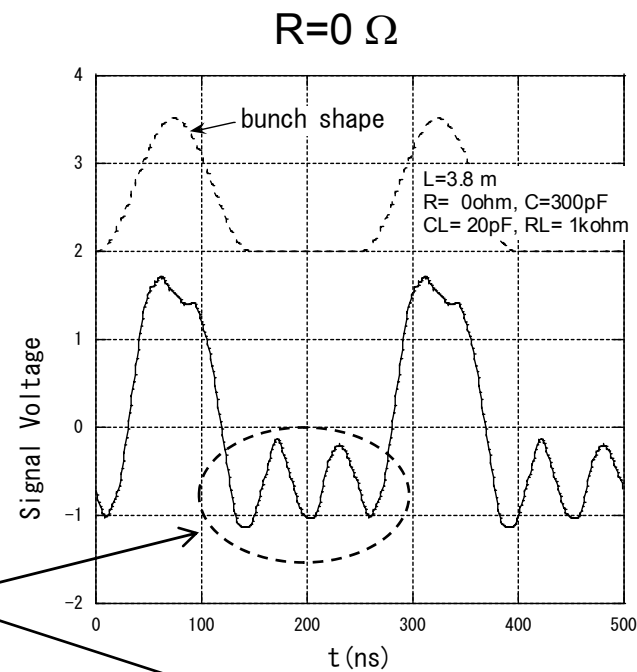
$$V(\omega) = G(\omega) \frac{Q(\omega)}{C}$$

To reproduce bunch shape in the observed signal V, R_L is required
to be $R_L C \gg$ (bunch length in time) for electrostatic pickup.
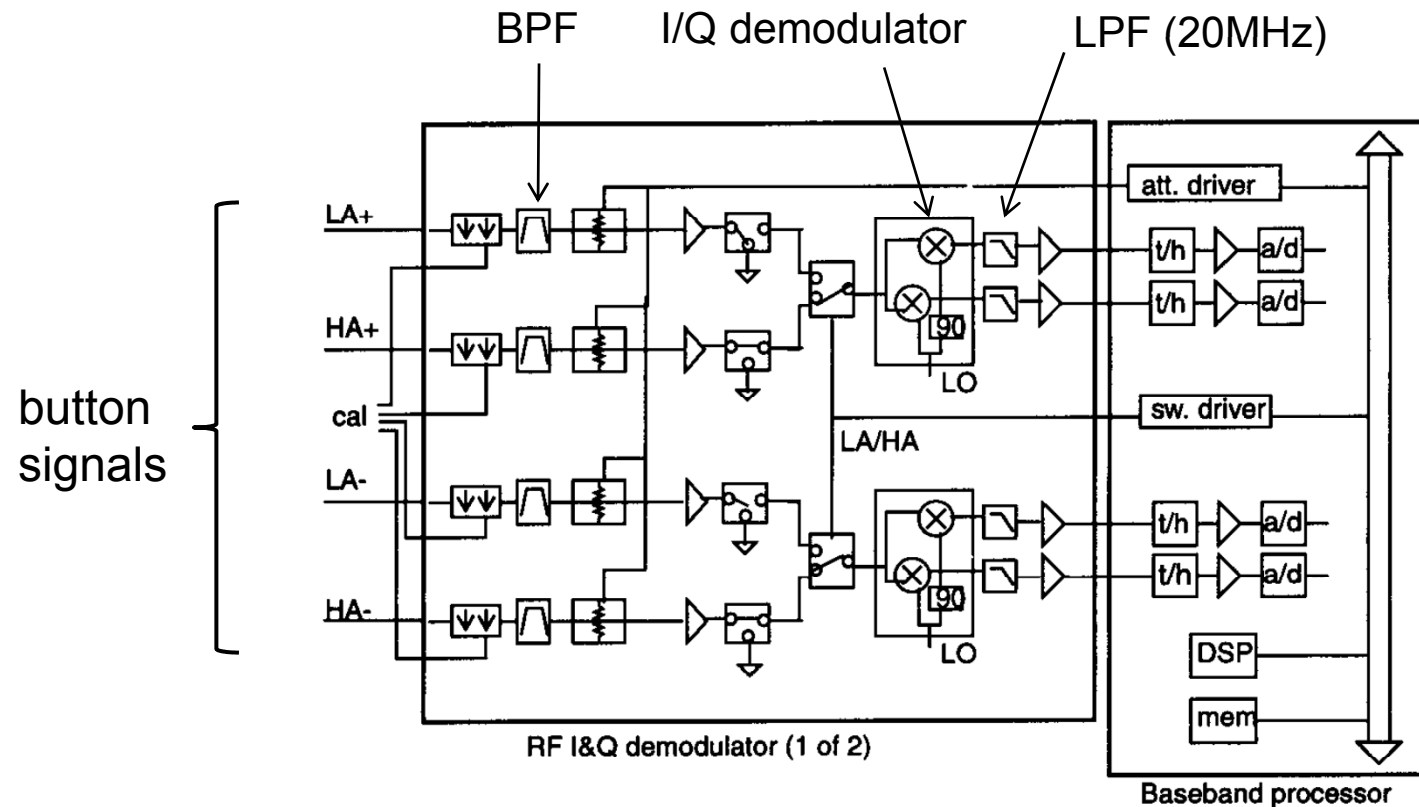High R_L causes signal cable resonance.
R connecting between the pickup electrode and the cable is effective
to damp the resonance (R=50-100Ω for Z_0=50Ω).

R=0 Ω

R=100 Ω

Resonance by
C and the reactance
of the cable loaded
with R_L and C_L.

L=3.8 m
R= 0ohm, C=300pF
CL= 20pF, RL= 1kohm

L=3.8 m
R=100ohm, C=300pF
CL= 20pF, RL= 1kohm

Δ/Σ processing at PEPII

C. Roberto et al.

BPF   I/Q demodulator   LPF (20MHz)

Signal bandwidth is designed to be 20 MHz for turn-by-turn measurement with 20 nsec sampling.
Measurement bandwidth is programable by DSP.

Δ/Σ processing at KEKB
(narrow bandwidth)

The signal frequency is down converted to the IF by a super-heterodyne.
In order to avoid errors caused by analog processing to detect signal amplitude,
IF signal is directly digitized and the spectrum amplitude of the beam signal
is detected by FFT in the DSP.
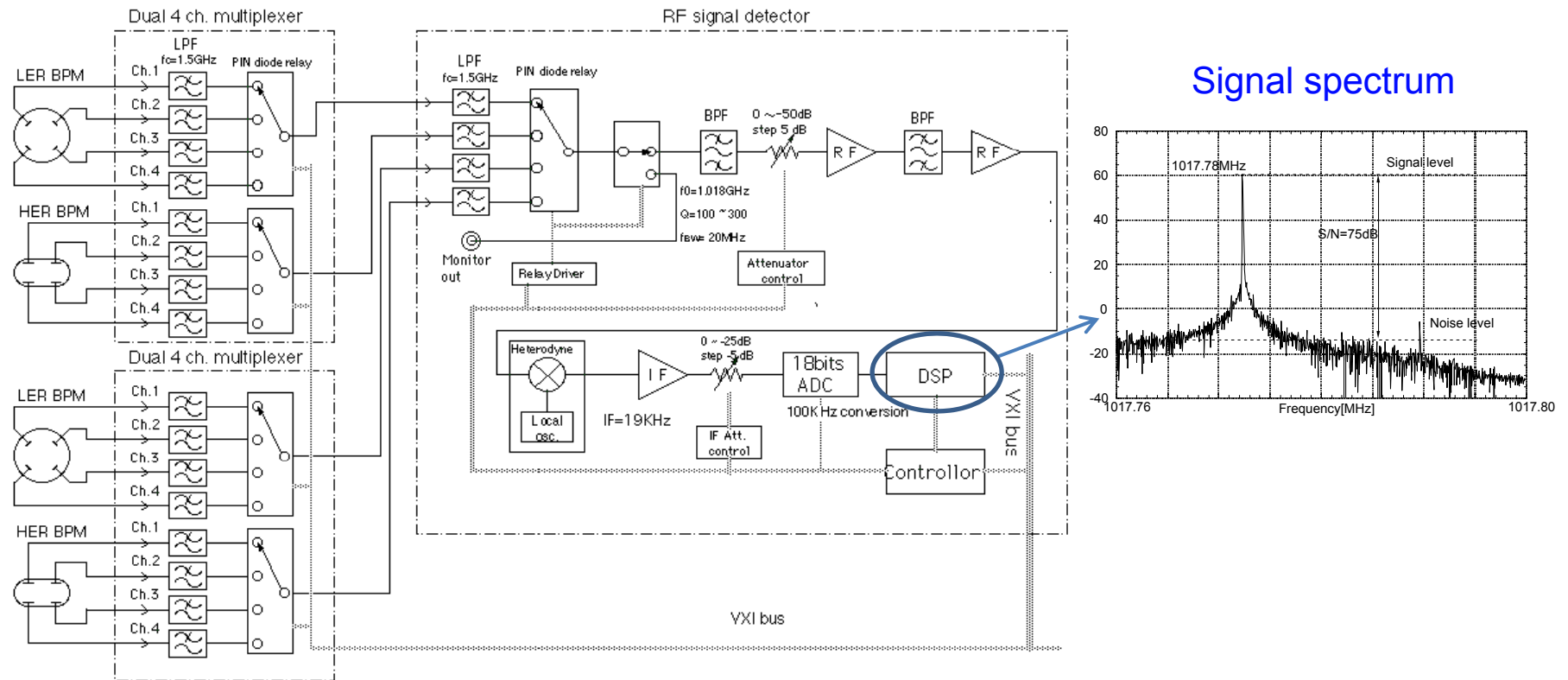
Signal spectrum

Δ/Σ processing at Jparc
(wide bandwidth: 10MHz)
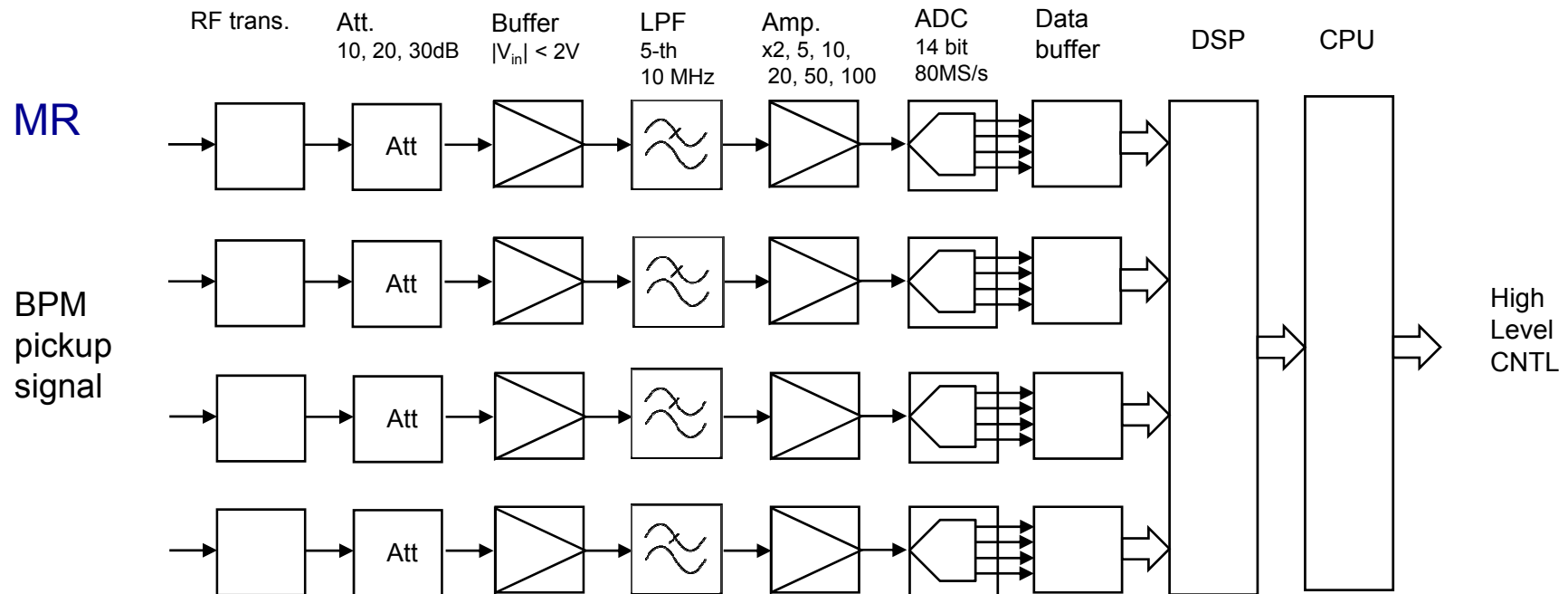
Each electrode signal is directly digitized.
The spectrum amplitude of the beam signal is detected by FFT
in the DSP.

Log-ratio BPM

F. D. Wells et al.

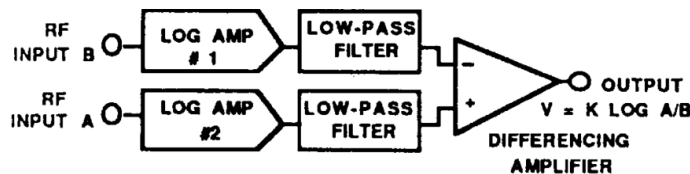$$V_{out} = K \ln \frac{A}{B} = 2K \tanh^{-1} \frac{A-B}{A+B}$$
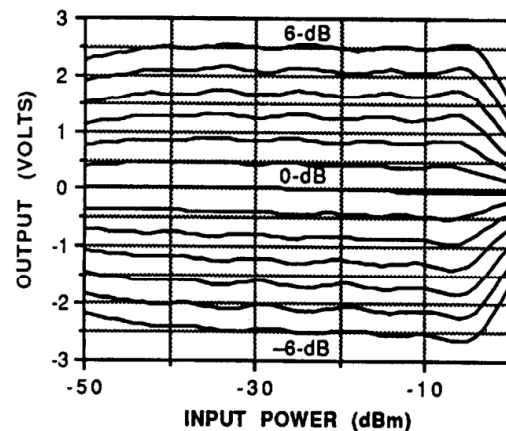

Figure 2. The log-ratio circuit block diagram.

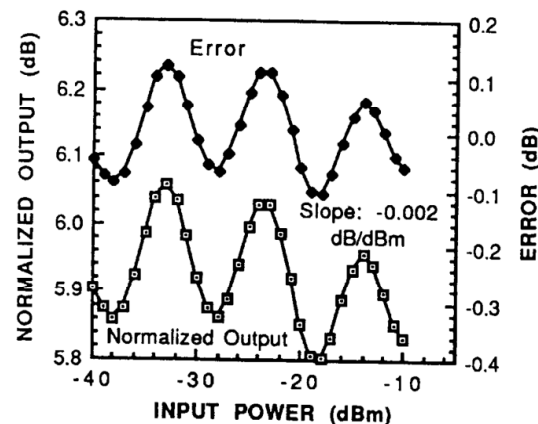Figure 4. Log-ratio circuit transfer function curves for 60 MHz rf input signals.

Figure 6. Error and normalized output curves for the 6-dB line of Figure 3.

- Output signal is more linear than Δ/Σ for parallel electrode pickup.

- Normalized beam position signal is obtained in real time.
  ---- Available for real time feedback

- Gain ripple of the log-amplifier against the input signal level causes the beam position error of about ~1%.
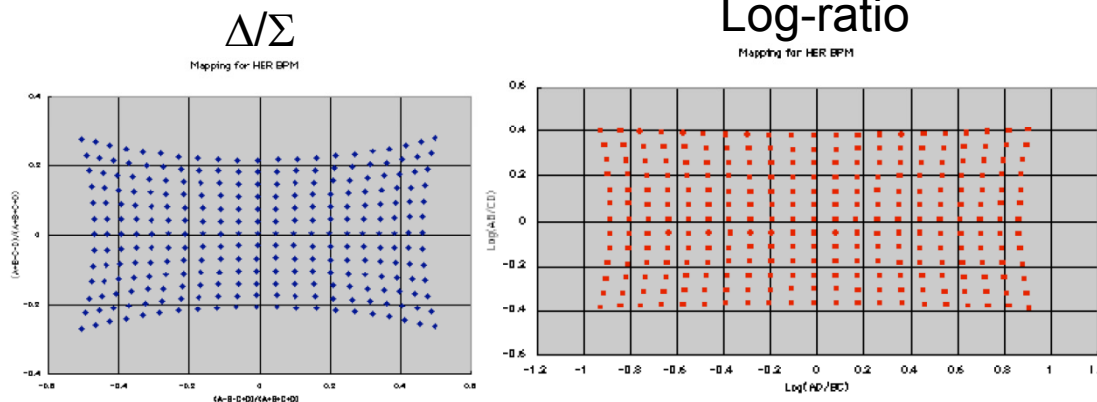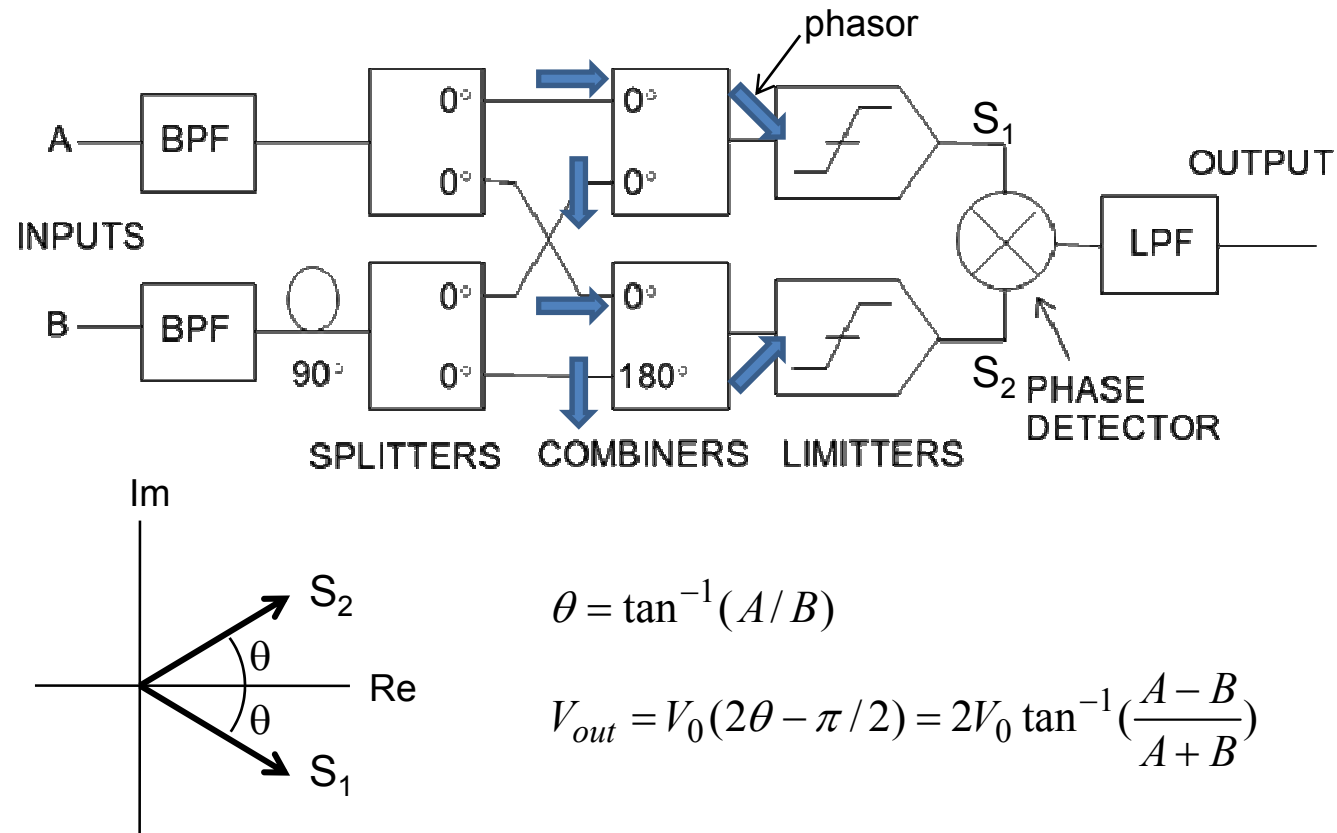
Log-ratio BPM at KEKB   M. Tejima
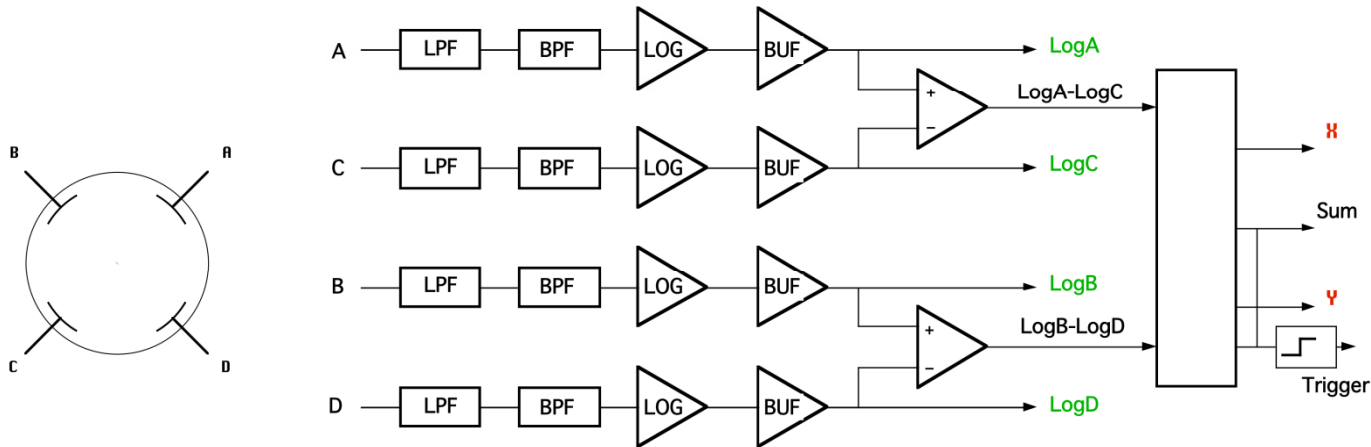
$$X = \log(A/C) - \log(B/D), \quad Y = \log(A/C) + \log(B/D)$$

BPM mapping (KEKB/HER BPM)

Δ/Σ Log-ratio

Improved nonlinearity by log-ratio processing.

AM-PM conversion processing

phasor

A — BPF ... 0° → 0° → S₁ ⟶ OUTPUT

INPUTS

B — BPF ... 90° 0° / 0° 180° → S₂ PHASE DETECTOR

SPLITTERS COMBINERS LIMITTERS

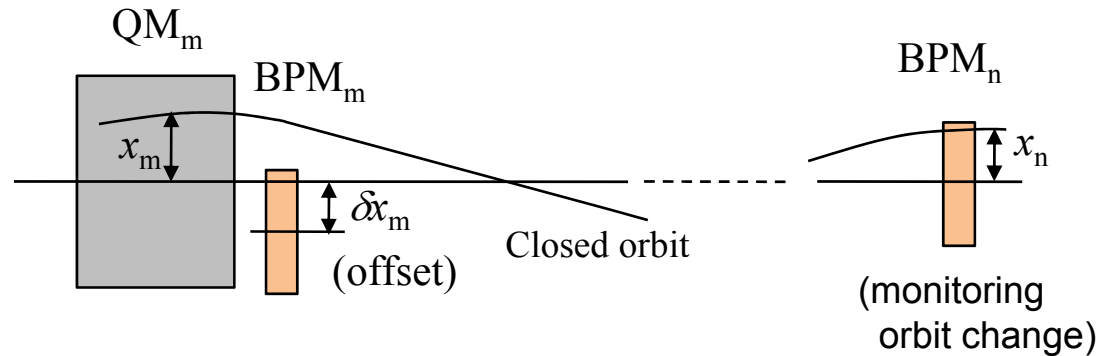$$\theta = \tan^{-1}(A/B)$$

$$V_{out} = V_0(2\theta - \pi/2) = 2V_0 \tan^{-1}(\frac{A-B}{A+B})$$

Big technical difficulty to make the system with high precision.
Large dynamic range and high real-time bandwidth can be expected.
(R. E. Shafer)

Beam based characterization of BPMs

Beam based alignment (BBA) of BPM

$$\Delta x_n = -a_{nm}(x_m - \delta x_m)\Delta K_m \ell$$

$$a_{nm} = \frac{\sqrt{\beta_n \beta_m}}{2\sin \pi \nu}\cos(\pi \nu - |\phi_n - \phi_m|)$$

Beam orbit x_n at BPM_n changes for $x_m \neq 0$ by changing QM_m strength ΔK_m.

Find out the beam orbit x_n unchanged by ΔK_m with steering magnets.

The beam orbit unchanged by ΔK_m is the center orbit of the QM_m.

The measured beam position by BPM_m is the BPM_m offset δx_m.

Beam based alignment (BBA)
J-Parc 50 GeV Ring

T. Toyama

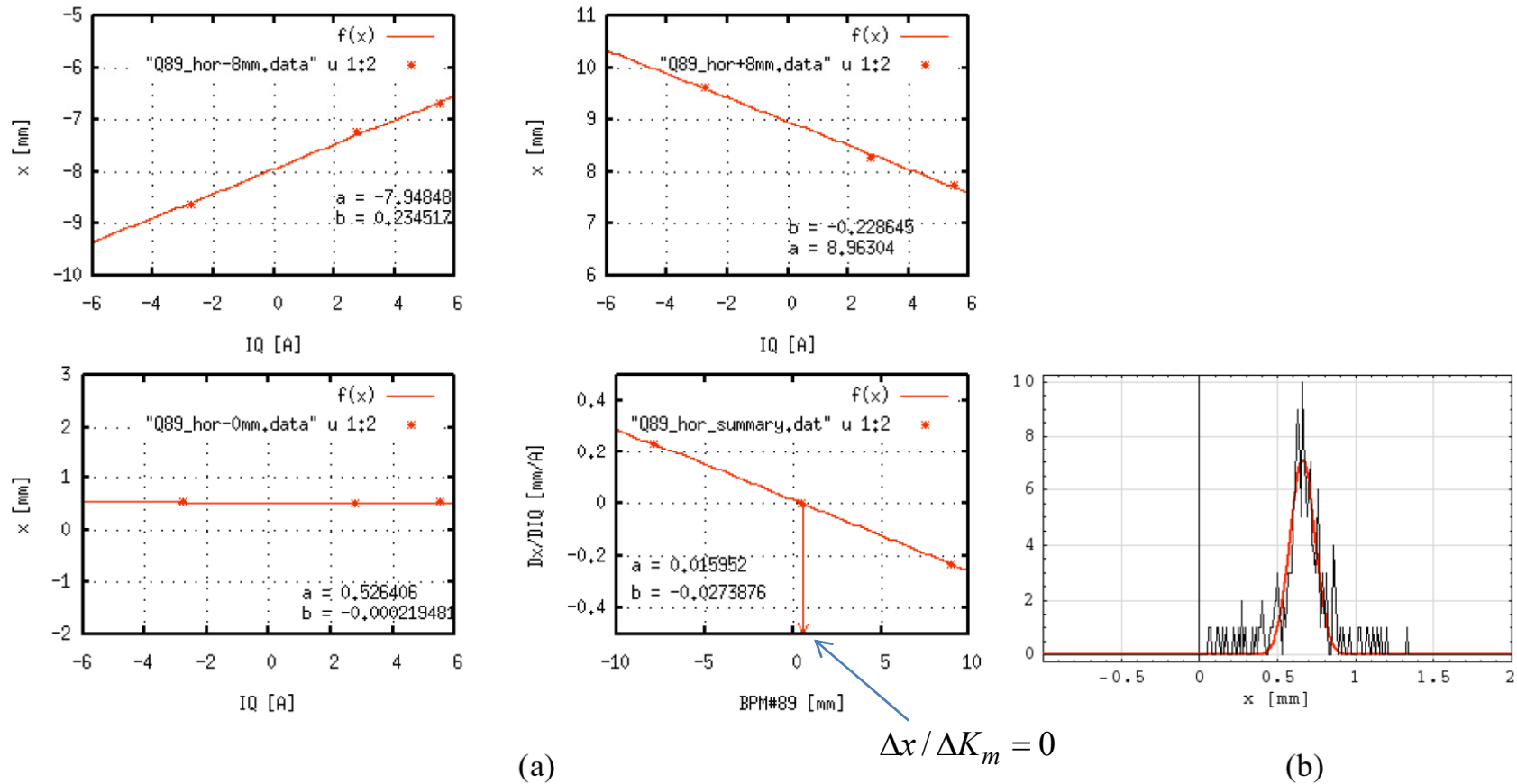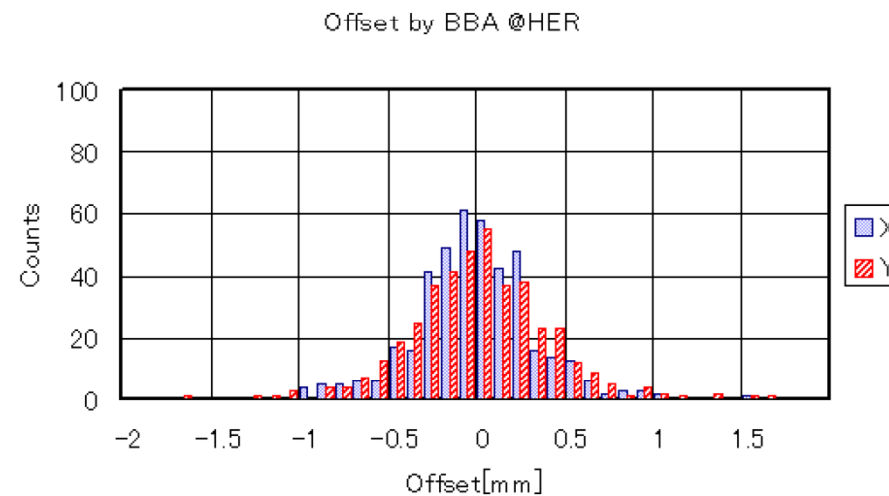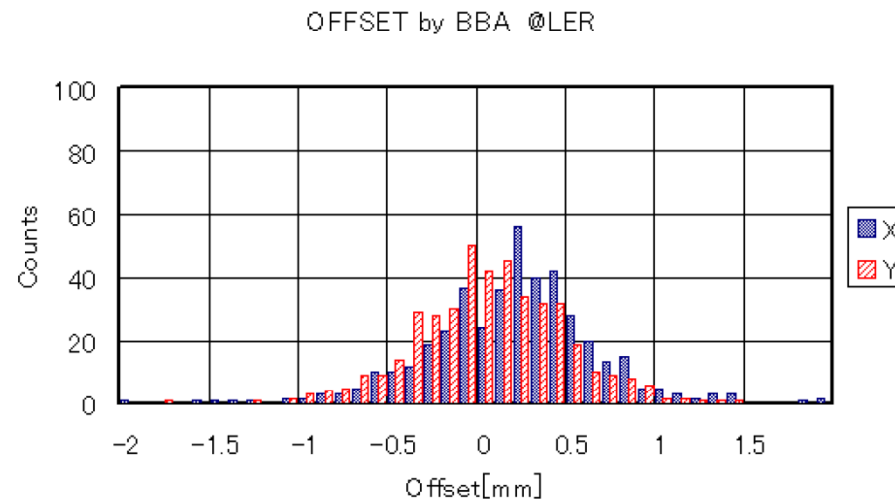$$\Delta x / \Delta K_m = 0$$

(a)

(b)

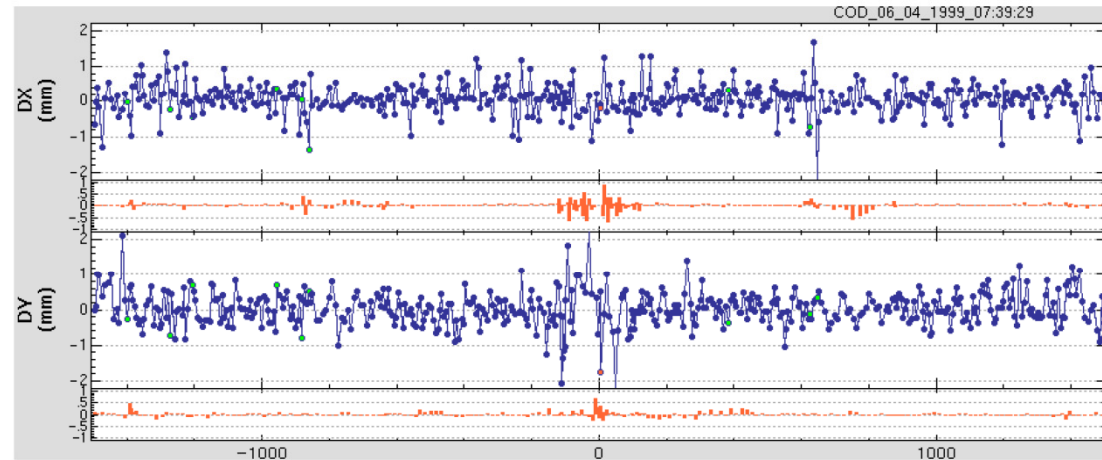Figure 7: Result of the Beam Based Alignment. (a) analysed using BPM89 only, (b) using all BPM's.
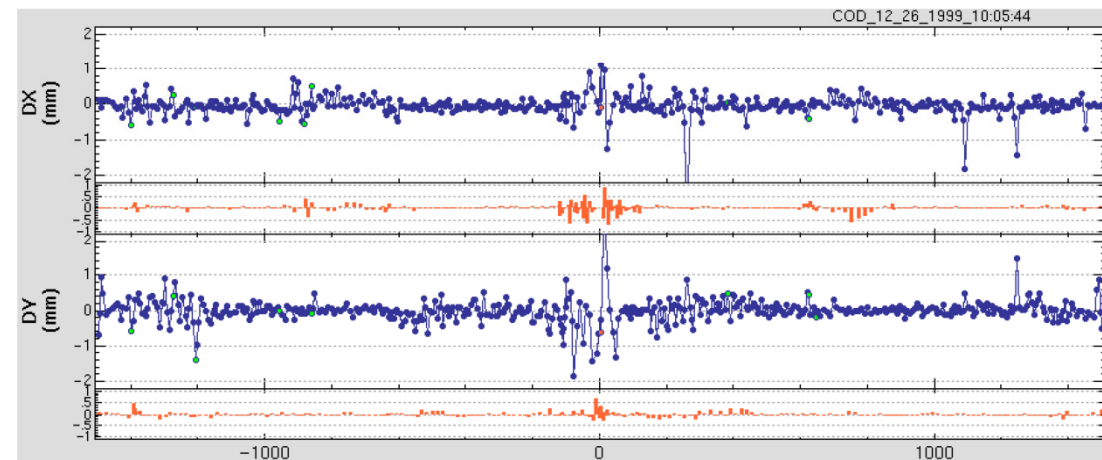
BPM offsets measured by BBA
KEKB LER & HER

M. Tejima

COD change by BBA (KEKB/LER)

w/o BBA

BBA

w/ BBA

Beam based pickup gain calibration of 4 button pickups (KEKB)

M. Tejima

Button signal response for the beam position (x,y) :

$$F_1(x,y) = 1 + a_1 x + b_1 y$$
$$+ a_2(x^2 - y^2) + b_2(2xy)$$
$$+ a_3(x^3 - 3x^2 y) + b_3(3xy^2 - y^3)$$
$$+ a_4(x^4 - 6x^2 y^2 + y^4) + b_4(x^3 y - xy^3)$$
$$+ \cdots\cdots$$

$$\begin{cases} F_2(x,y) = F_1(-x,y), & F_3(x,y) = F_1(-x,-y) \\ F_4(x,y) = F_1(x,-y) \end{cases}$$
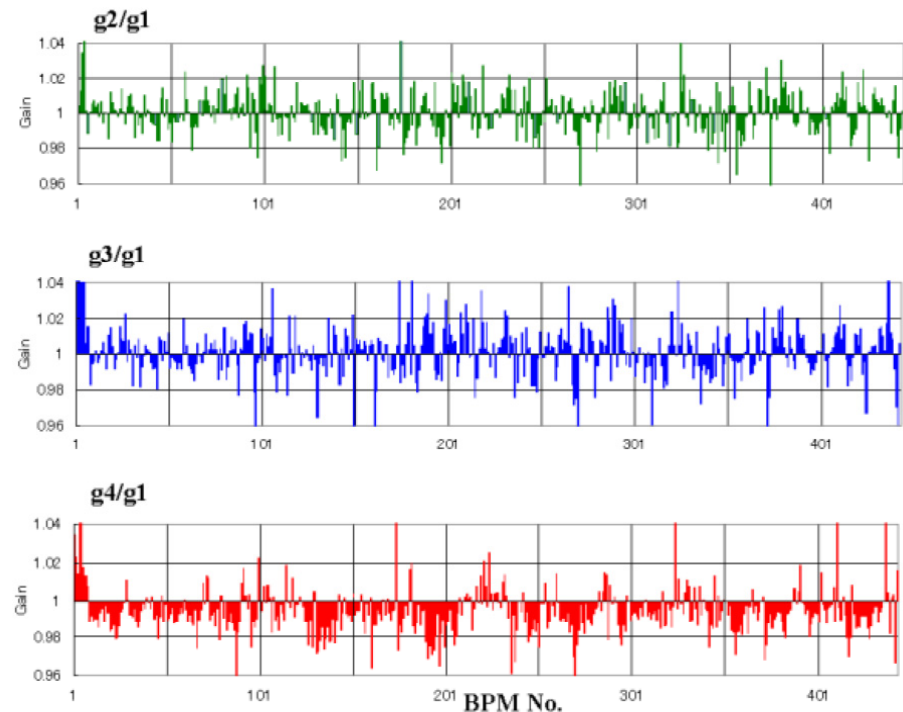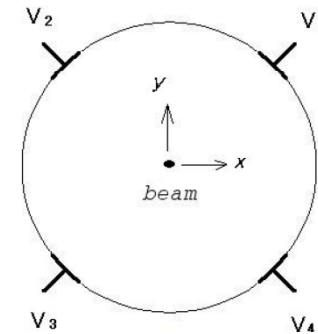
i-th button signal at j-th measurement :

$$V_{ij} = g_i q_j F_i(x_j, y_j) \qquad \begin{cases} i = 1, \cdots, 4 \\ j = 1, \cdots, m \end{cases}$$

$$J = \sum_{i=1}^{4} \sum_{j=1}^{m} \{ V_{ij} - g_i q_j F_i(x_j, y_j) \}^2$$
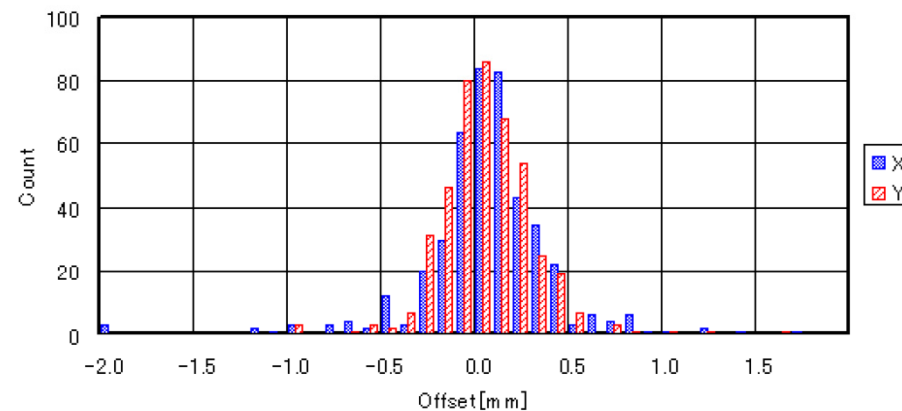
Least squares of J give :

$$\begin{cases} g_2/g_1, \cdots, g_4/g_1 \\ q_1, \cdots, q_m, x_1, \cdots, x_m, y_1, \cdots, y_m \end{cases}$$
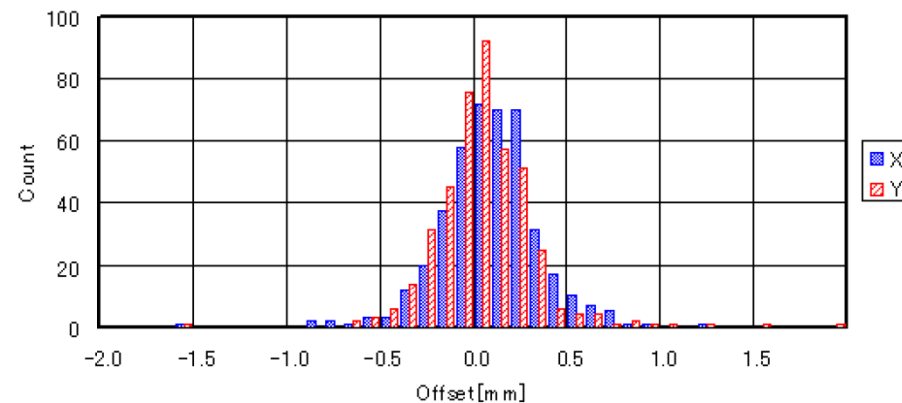
BPM offsets after beam based gain calibration (measured by BBA, KEKB LER & HER)

M. Tejima

After gain correction, offset by BBA @ LER

After gain correction, offset by BBA @ HER

BPM offsets by imbalance of pickup electrode gains(KEKB)

BPM offset (w/o beam based gain calibration)

	LER(horizontal/vertical)	HER(horizontal/vertical)
average	0.110/-0.025 mm	-0.097/-0.085 mm
σ	0.49/0.43 mm	0.34/0.40 mm

BPM offset (w/   beam based gain calibration)

	LER(horizontal/vertical)	HER(horizontal/vertical)
average	-0.026/-0.034 mm	-0.005/-0.052 mm
σ	0.374/0.254 mm	0.272/0.254 mm

Beam based gain calibration of diagonal cut BPM (J-Parc)

T. Toyama

The equation is written by

$$Ax = b$$

$$A = \begin{pmatrix} -V_{R1} & V_{U1} & V_{D1} \\ -V_{R2} & V_{U2} & V_{D2} \\ \vdots & \vdots & \vdots \\ -V_{Rn} & V_{Un} & V_{Dn} \end{pmatrix}, \quad x = \begin{pmatrix} 1/g_R \\ 1/g_U \\ 1/g_D \end{pmatrix}, \quad b = \begin{pmatrix} V_{L1} \\ V_{L2} \\ \vdots \\ V_{L_n} \end{pmatrix}$$

A and b have errors $\rightarrow$ Total least squares method

Least squares solution :

$$x_{LS} = (A^T A)^{-1} A^T b$$

Total least squares solution

$$x_{TLS} = (A^T A - \sigma_{n+1}^2 I)^{-1} A^T b$$

σ_{n+1} is the smallest singular valure of $[A \ \ b]$

• Good reproduction of gain erros with TLS is confermed by simulation.

$$\begin{cases} V_L = \lambda \cdot \left(1 + \dfrac{x}{a}\right), \quad V_R = g_R \cdot \lambda \cdot \left(1 - \dfrac{x}{a}\right) \\ V_U = g_U \lambda \cdot \left(1 + \dfrac{y}{a}\right), \quad V_D = g_D \cdot \lambda \cdot \left(1 - \dfrac{y}{a}\right) \end{cases}$$

$$V_{Lj} = -\frac{1}{g_R} V_{Rj} + \frac{1}{g_U} V_{Uj} + \frac{1}{g_D} V_{Dj}, \quad j = 1, \cdots, m$$

$$\begin{pmatrix} -V_{R1} & V_{U1} & V_{D1} \\ & \vdots & \\ -V_{Rj} & V_{Uj} & V_{Dj} \\ & \vdots & \\ -V_{Rm} & V_{Um} & V_{Dm} \end{pmatrix} \begin{pmatrix} \dfrac{1}{g_R} \\ \dfrac{1}{g_U} \\ \dfrac{1}{g_D} \end{pmatrix} = \begin{pmatrix} V_{L1} \\ \vdots \\ V_{Lj} \\ \vdots \\ V_{Lm} \end{pmatrix}$$

Beam based gain calibration with LS and TLS.

Table 2: Test of Beam Based Gain Calibrations

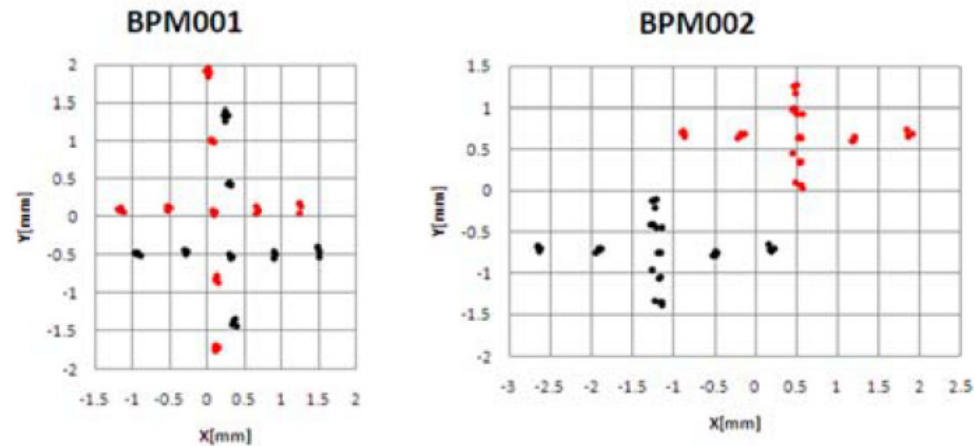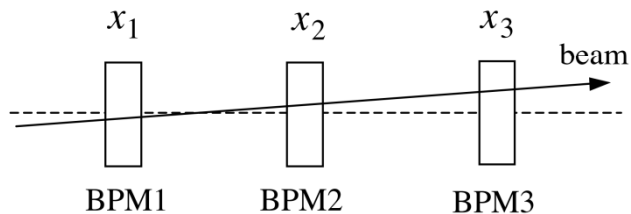| BPM001	g_2	g_3	g_4
TLS	1.0062	1.0024	0.9873
LS	1.0103	1.0045	0.9892
BPM002	g_2	g_3	g_4
TLS	0.9568	0.9811	0.9463
LS	0.9617	0.9838	0.9487

Figure 5: Reconstructed mapping data. Red: (x, y) without correction, Black: (x, y) with TLS.

Resolution of BPM system
(3-BPM correlation method)

T. Toyama

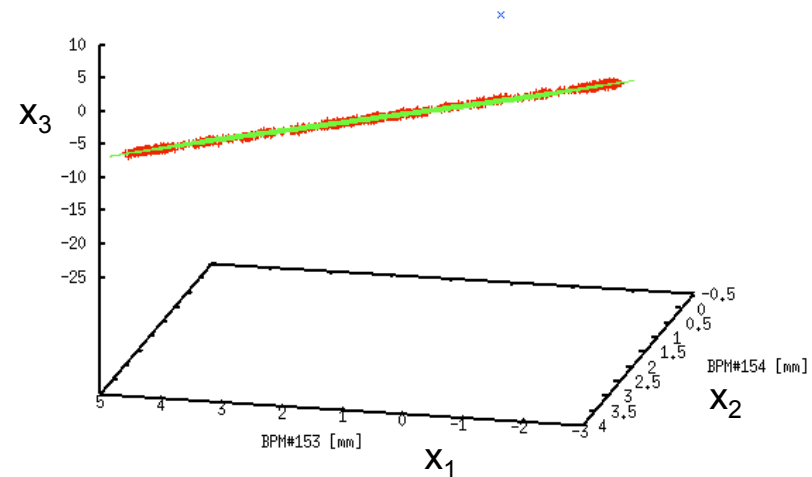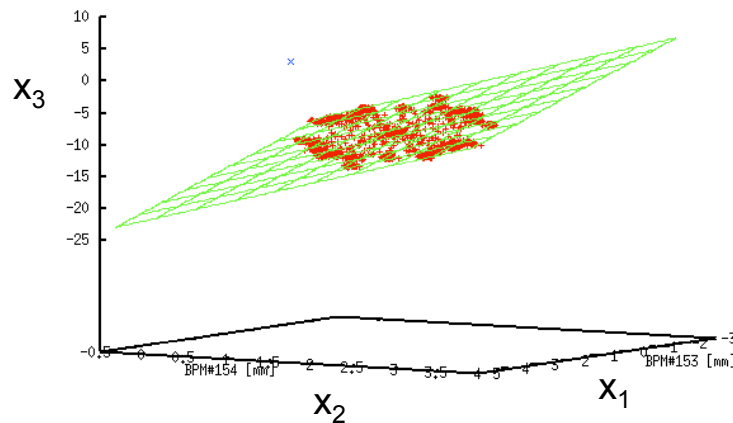$$x_3 = Ax_1 + Bx_2 + C$$

x_1　x_2　x_3

beam

BPM1　　BPM2　　BPM3

A, B, C are determind by minimizing

$$F^2 = \sum_i \{x_{3,i} - (Ax_{1,i} + Bx_{2,i} + C)\}^2$$

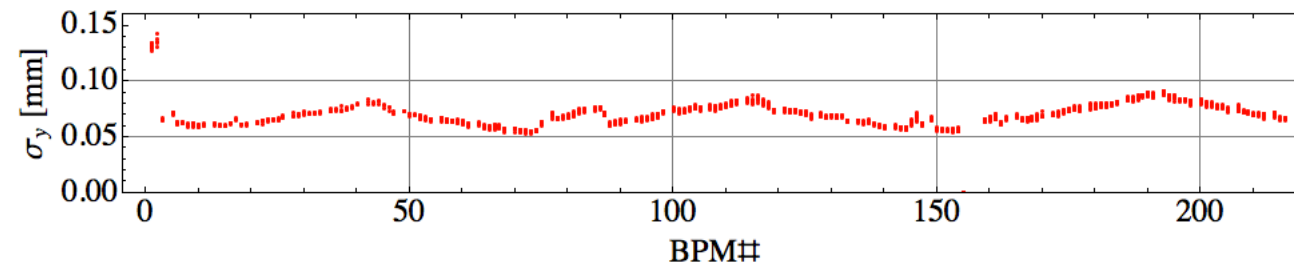Assuming same resolution of 3 BPMs, the resolution is given by

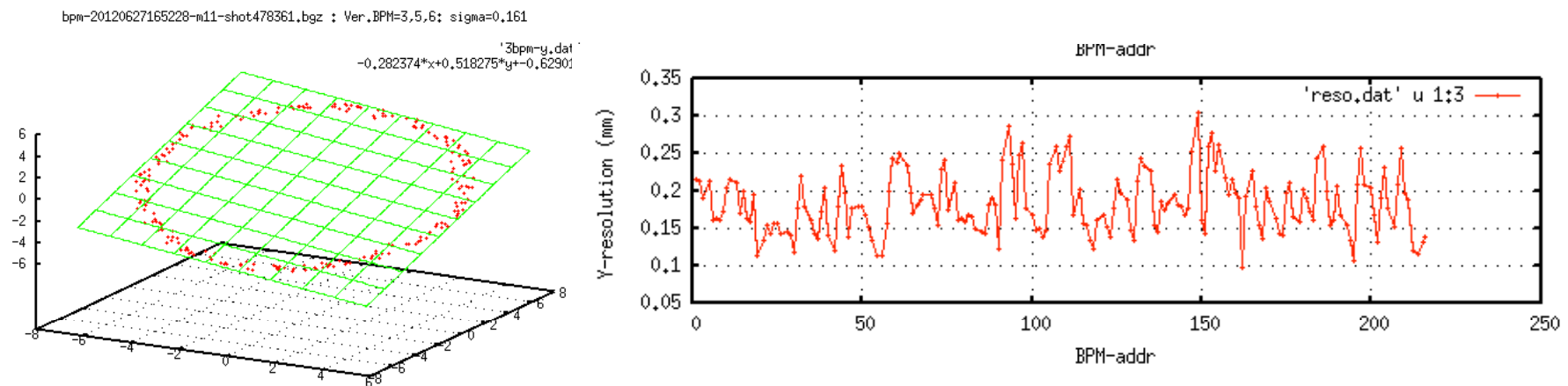$$\sigma = \sqrt{\frac{1}{N-1} \frac{\sum_i^N \{x_{3,i} - (Ax_{1,i} + Bx_{2,i} + C)\}^2}{1 + A^2 + B^2}}$$

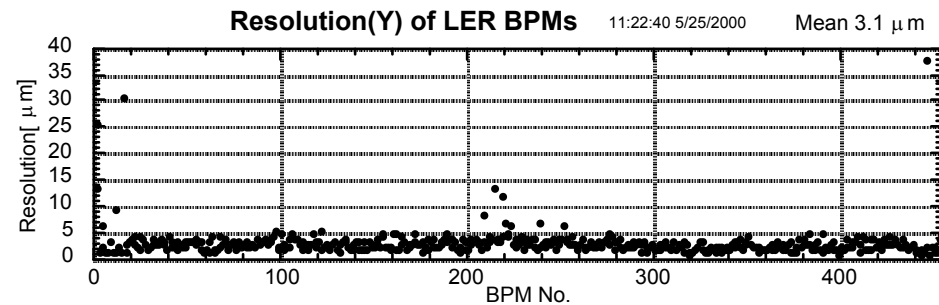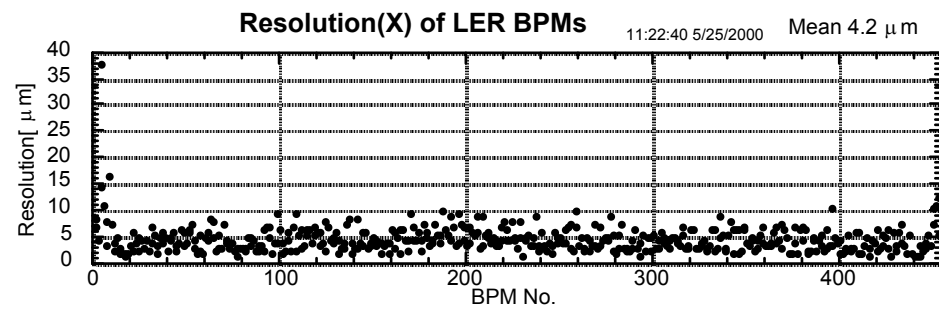# Measured BPM resolution of J-Parc MR

T. Toyama

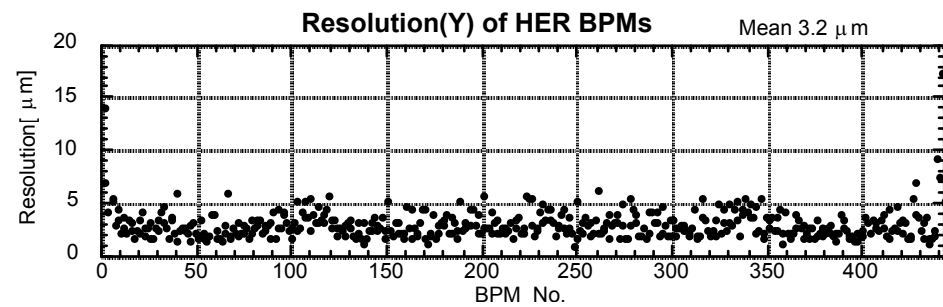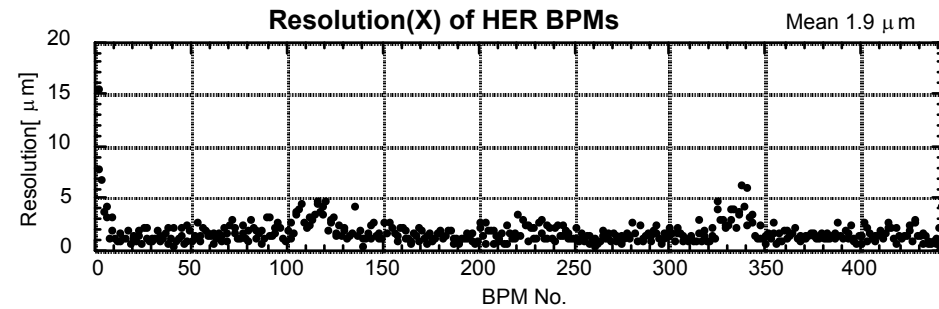Measured resolution in normal mode (narrow bandwidth)

Resolution in single-pass mode (wide bandwidth)
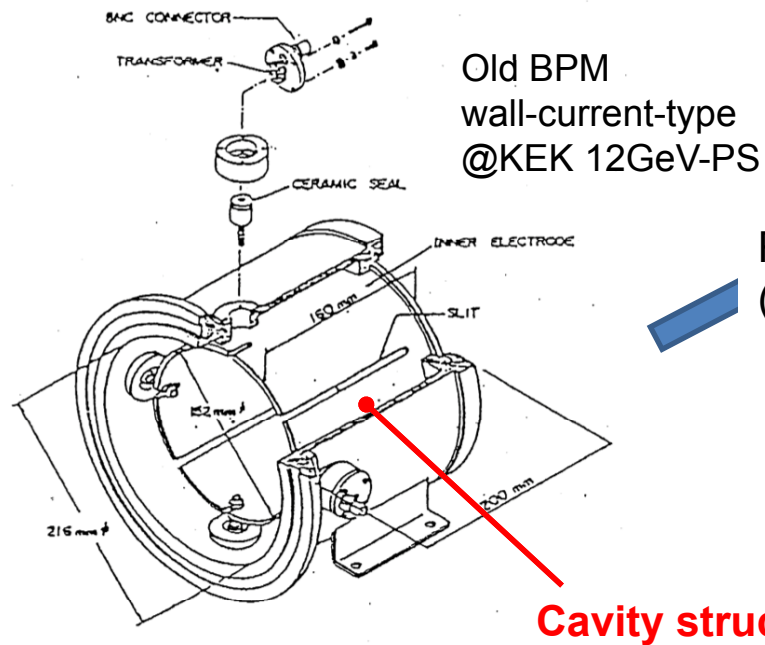
Measured BPM
resolution of KEKB
(3 BPMs mehod)

Resolution(X) of HER BPMs Mean 1.9 μm

Resolution(Y) of HER BPMs Mean 3.2 μm

Resolution(X) of LER BPMs 11:22:40 5/25/2000 Mean 4.2 μm

Resolution(Y) of LER BPMs 11:22:40 5/25/2000 Mean 3.1 μm

Coupling impedance of BPM pickups

BPM impedance reduction (KEK 12GeV PS)
BPM impedance affected the instability

T. Toyama

Old BPM
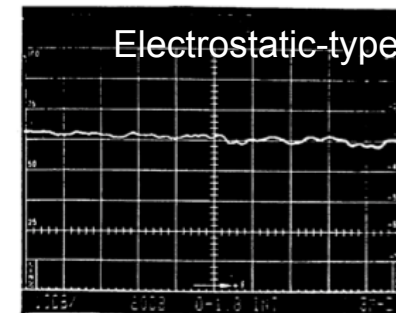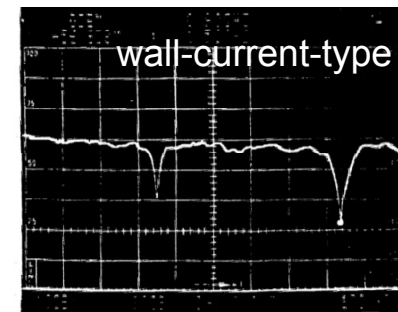wall-current-type
@KEK 12GeV-PS

Replaced
(1997)

Cavity structure

Electrostatic-type BPM with 4 electrodes
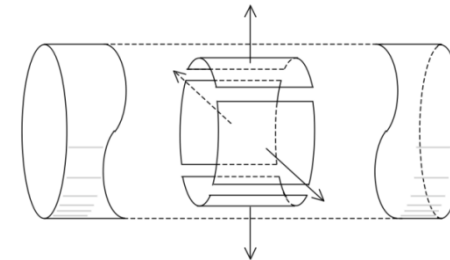
Measured transmission S_{21} with coaxial-line
f = 0 – 1.8 GHz, 10dB/div

wall-current-type

Electrostatic-type

Resonant impedance (measured/calculation) of WCM-type BPM

	$\omega/2\pi$ (GHz)	Q	R_{shunt} (Ω)	R/Q (Ω)
BPM	0.636/0.667 1.498/1.377	77/2650 230/8222	$1.5\times10^3/2.6\times10^4$ $5.3\times10^3/3.3\times10^4$	19.4/9.8 23/40

K. Takayama *et al*. Phys. Rev. Lett. 78 (1997) p.871

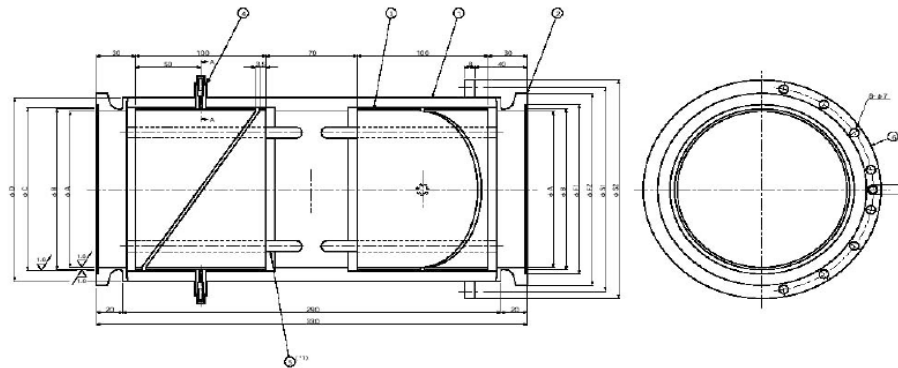D. Arakawa, in KEK Proceedings 98-1 (*Japanese*)

Replacement of wall-current-type BPMs to electrostatic-type BPMs improved longitudinal emittance blow-up. (KEK 12GeV PS)
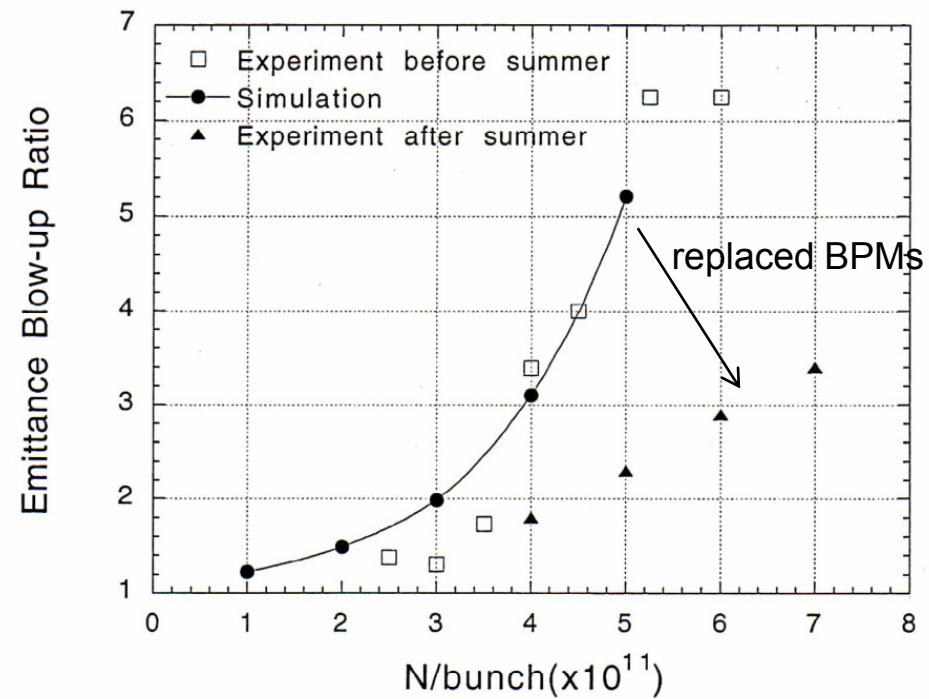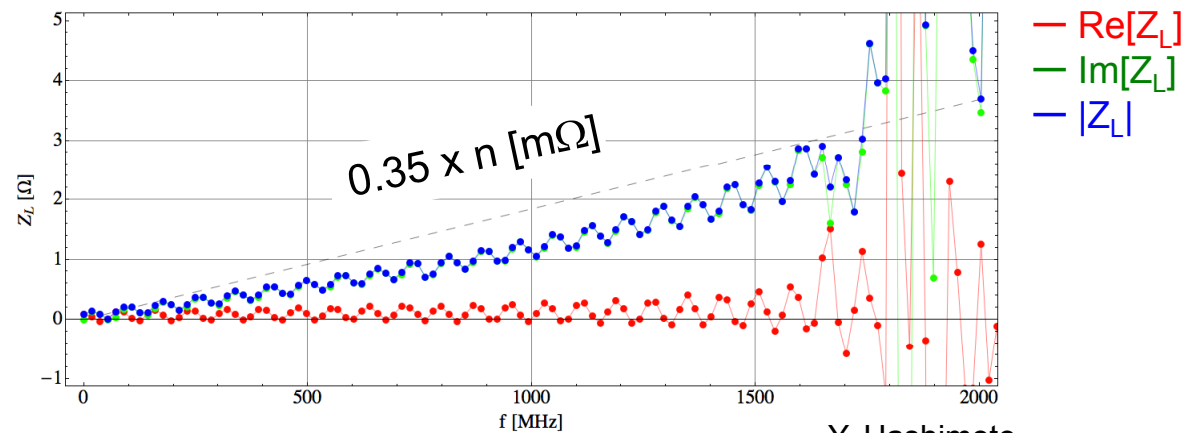

Longitudinal emittance vs. beam intensity

Broadband impedance of diagonal cut BPM (J-PARC, MR)

T. Toyama

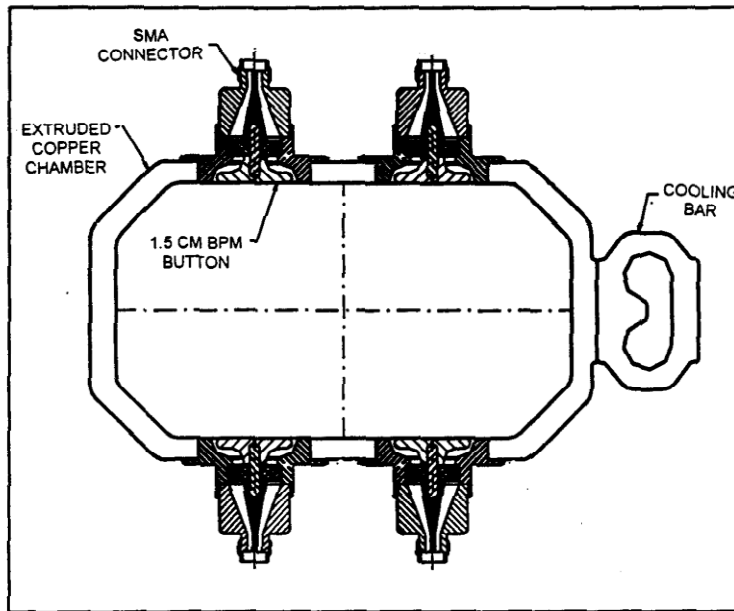Simulation results by **CST PARTICLE STUDIO(R)**

Y. Hashimoto

No significant resonance, $|Z_L/n| < 0.35 \times 186\ m\Omega = 65\ m\Omega \ll 9\ \Omega_{max}$ (Keil-Schnell criterion)

Y.Shobuda

Coupling impedance of SLAL PEPII BPM

C. –K. Ng et al.

3D EM field calculation with MAFIA

PEPII BPM with 15mmϕ buttons

Energy loss by beam	126 W
Power out of one cable	9 W (37 W)*
Transfer impedance at 1 GHz	0.65 Ω
Broad-band impedance, $|Z/n|$	0.008 Ω (11 nH)
Narrow-band MAFIA	6.5 kΩ at ~ 6.8 GHz
impedance: accepted	3.4 kΩ

Resonant impedance of a BPM
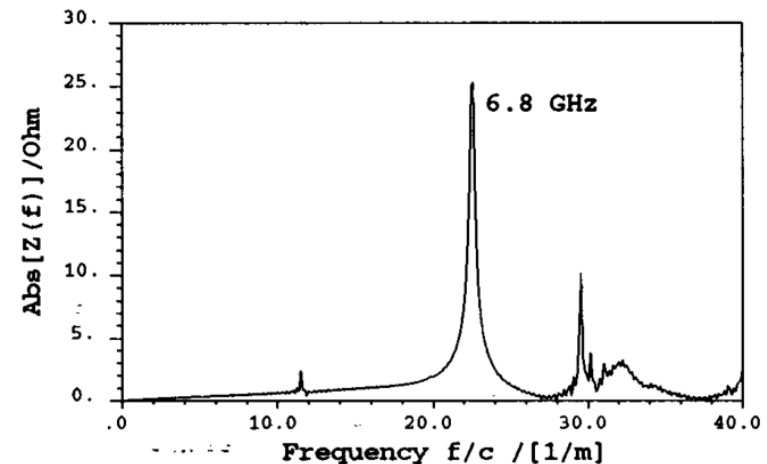

Acceptable impedance is determined so that the maximum growth rate of coupled-bunch instabilities does not exceed the radiation damping rate.
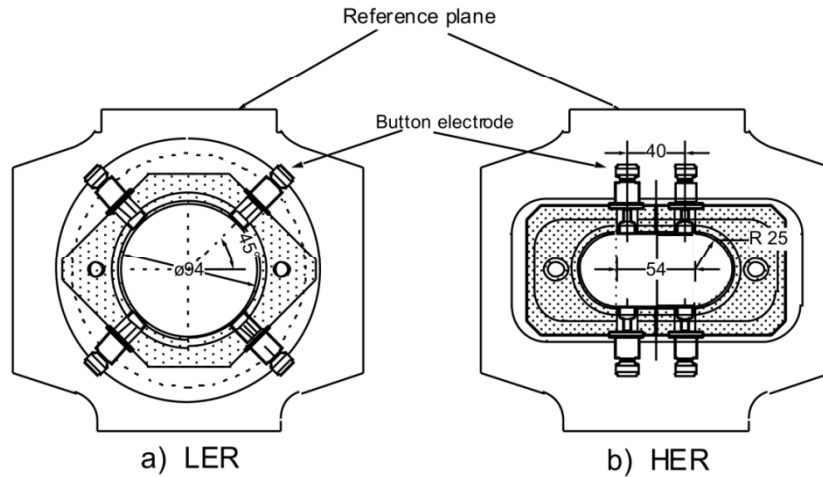
Resonant Impedance of KEKB BPMs

N. Akasaka
K. Shibata

a) LER

b) HER

Growth rate of multibunch instability

$$\tau_\mu^{-1} = \frac{e\alpha I}{2ET\omega_s} \sum_{p=1}^{\infty} \left[\omega_p^{(\mu+)} \rho(\omega_p^{(\mu+)}) \mathrm{Re}\{Z(\omega_p^{(\mu+)})\} \right.$$

$$\left. -\omega_p^{(\mu-)} \rho(\omega_p^{(\mu-)}) \mathrm{Re}\{Z(\omega_p^{(\mu-)})\} \right]$$

$$Z(\omega) = NR_s / \{1 + iQ(\omega_R/\omega - \omega/\omega_R)\}$$

$$\boxed{\tau_\mu^{-1} < \tau_R^{-1} \,(\text{damping rate by SR})}$$

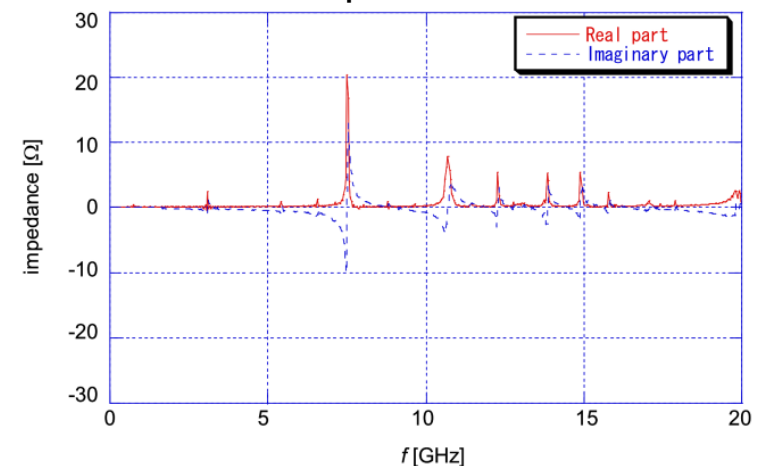➡ Acceptable beam current I_{max}

Resonant impedance

Acceptable current
(by 4-buckets filling)

	f_R (GHz)	R_s (Ω)	NR_s (kΩ)	Q	I_{max} (A)
LER	7.61	8.1	3.6	137	1.6
HER	7.57	17.4	7.7	91	2.4

Broad-band impedance $|Z_{//}/n|$: 0.0014 Ω (LER)
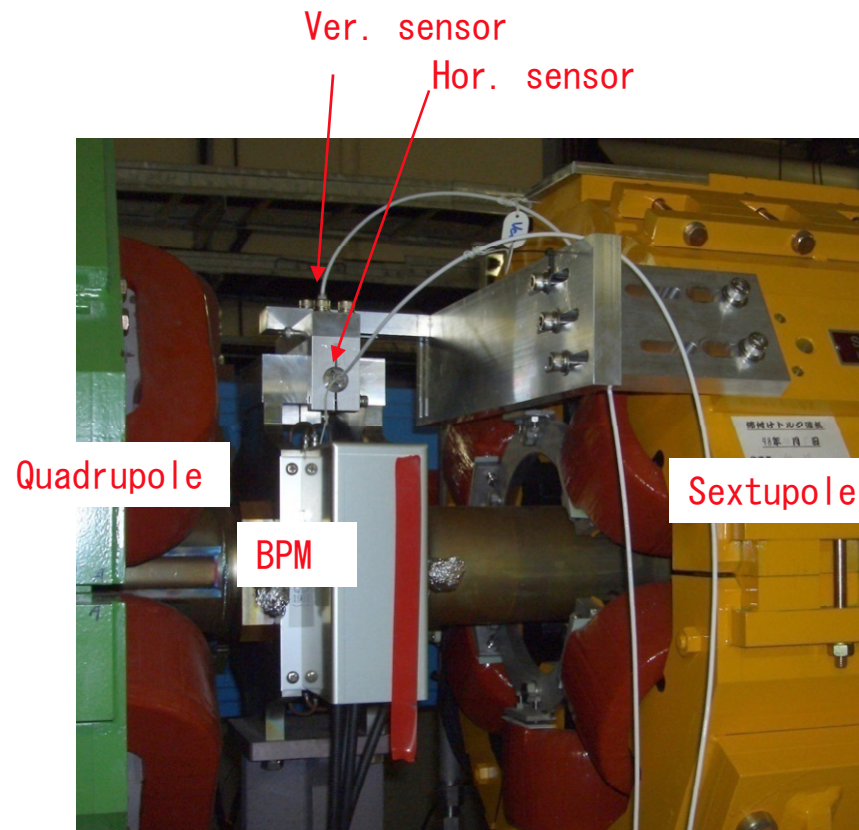0.004 Ω (HER)

(N. Akasaka, K. Shibata)

Calculate impedance with MAFIA

Displacement of BPM pickups by thermal distortion of beam chambers (KEKB)
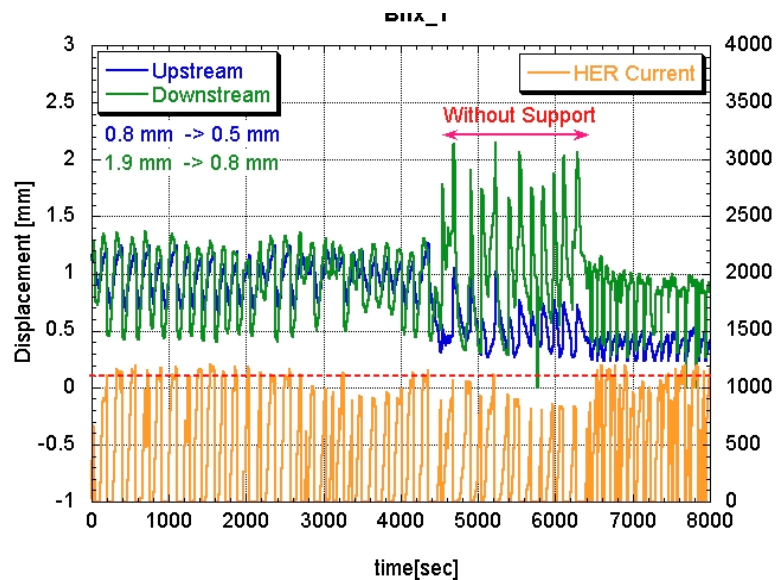
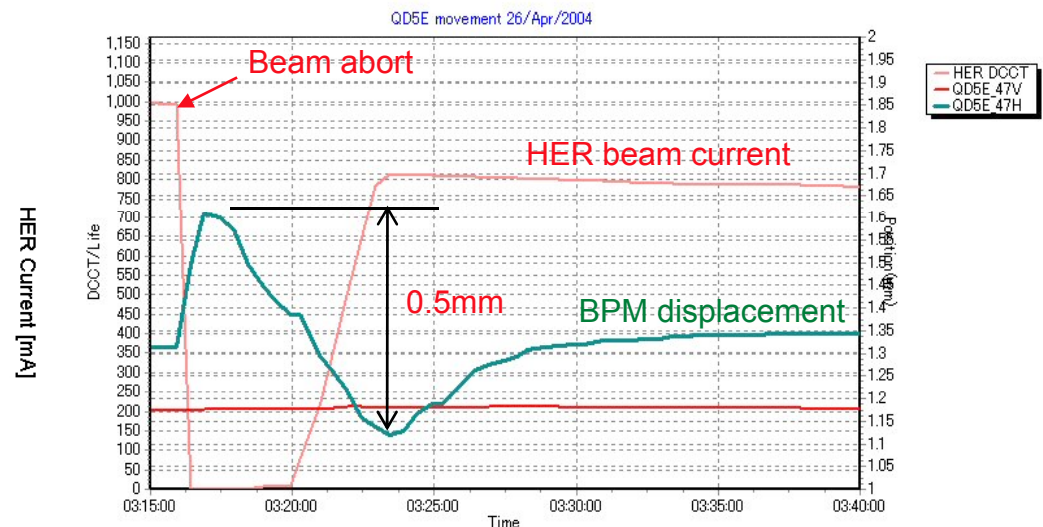# Displacement sensors for BPM pickups

BPM displacement sensors attached to the sextupole magnet

- BPM chambers are displaced from the setting position by beam pipe deformation due to the heating by strong irradiation of synchrotron radiation.
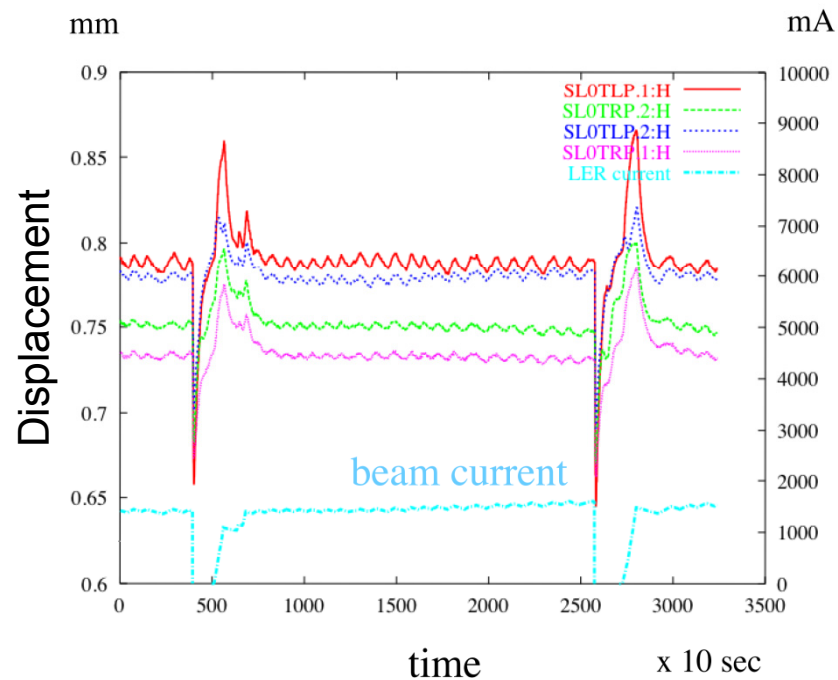
Displacement of bending chamber
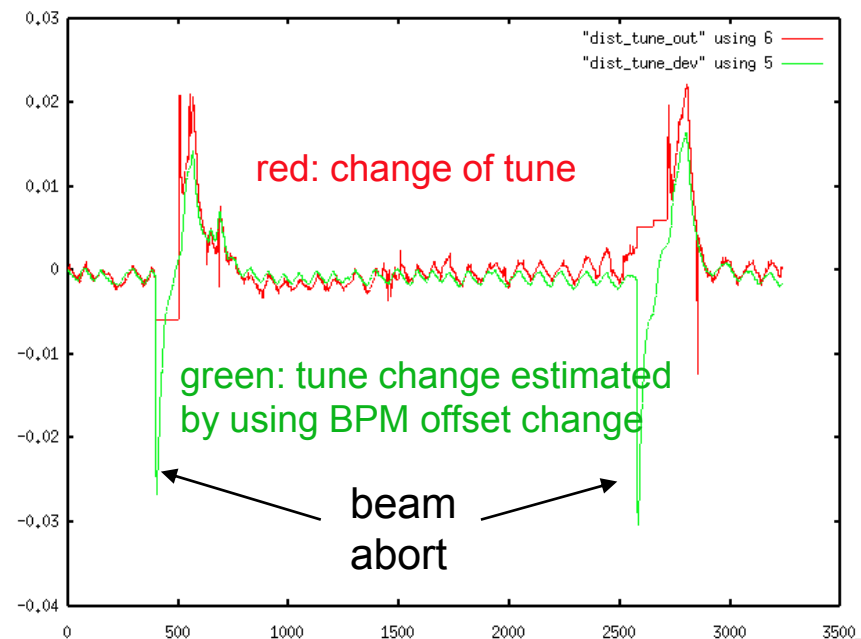
Movement of BPM pickup

Tune change by BPM displacement (KEKB)

H. Fukuma

Displacement of BPM pickups
against 6-pole magnets

LER vertical tune change

red: change of tune

green: tune change estimated
by using BPM offset change

beam
abort

BPM displacement occurs tune change.

Concluding remarks

- We have many issues to be considered for design and construction of the BPM system.

- It is one of the difficult problems to guarantee the precise measurement of beam positions for different operations of accelerators.

  For example the operation condition of accelerators at the commissioning stage or the machine study is very different from the routine operation.

- To guarantee the accuracy of the beam position measurements at various operation conditions, it is important to fully understand the beam diagnostic devices and also the accelerator facility.